A physics-based framework for modelling the performance and reliability of BIPV systems

Peer-reviewed author version

KAAYA, Ismail; Alzade, Abdella; BOUGUERRA, Sara; KYRANAKI, Nikoleta; BAKOVASILIS, Apostolos; RAMESH, Santhosh; Saelens, Dirk; DAENEN, Michael & MORLIER, Arnaud (2024) A physics-based framework for modelling the performance and reliability of BIPV systems. In: Solar Energy, 277 (Art N° 112730).

DOI: 10.1016/j.solener.2024.112730
Handle: http://hdl.handle.net/1942/43419

A Physics-based framework for modelling the performance and reliability of BIPV systems

Ismail Kaaya[a,b,c *], Abdella Alzade[d], Sara Bouguerra[a,b,c], Nikoleta Kyranaki[a,b,c], Apostolos Bakovasilis[a,b,c], Santhosh Ramesh[a,b,c], Dirk Saelens[d], Michaël Daenen[a,b,c], Arnaud Morlier[a,b,c]

[a]Imec, imo-imomec, Thor Park 8320, 3600 Genk, Belgium, [b]Hasselt University, imo-imomec, Martelarenlaan 42, 3500 Hasselt, Belgium Belgium, [c]EnergyVille, imo-imomec, Thor Park 8320, 3600 Genk, Belgium, [d] KU Leuven, Kasteelpark Arenberg 40, Leuven (Heverlee), Belgium

Abstract

Building-Integrated Photovoltaic (BIPV) systems usually operate under elevated temperatures and are under frequent shading in comparison to standard or ground installed PV systems. These operating conditions might positively or negatively influence the performance and reliability of BIPV systems components. This study introduces a comprehensive simulation framework designed to model and assess the performance and reliability of BIPV systems. The framework incorporates sub-models for buildings, energy yield, and PV module/inverter reliability, some of which are validated using experimental data from a BIPV demonstrator. Initially, we applied the framework to demonstrate the critical role of precisely estimating the micro-climate surrounding the BIPV system. This inclusion in the electrical/energy yield model, as opposed to relying solely on ambient climate conditions, significantly enhances modeling accuracy. Furthermore, the framework is employed to simulate the reliability implications of BIPV systems installed with and without ventilation. Our analysis reveals that a properly installed BIPV system with ventilation surpasses the 25-year module warranty in all studied climate zones. Conversely, systems without ventilation exhibit a substantial reduction in module lifetime, particularly in hot and dry, and hot and humid climates. Lastly, we employed the framework to assess the impact of shading on PV module reliability. While shaded BIPV systems demonstrated an improvement in module lifetime due to reduced climatic stressors, the gains were insufficient to offset energy losses from shading effects. Our proposed framework offers versatility for diverse "what if" simulations, enabling the evaluation of performance and reliability aspects of BIPV systems crucial for research and BIPV project bankability.

Keywords: BIPV, energy yield, reliability, climate zones, performance, modelling, PV system

1. Introduction

BIPV is a technology that integrates solar panels into the fabric of the building. This innovative approach not only generates electricity but also helps to reduce the building's energy consumption and carbon footprint. BIPV systems can be employed in both new constructions and retrofit projects and can be incorporated with other building components such as skylights, shading devices, and ventilated façades [1].

Table 1.Nomenclature

Abbreviations and Symbols	
DR_H	Hydrolyis degradation rate
DR_P	Photodegradation rate
DR_T	Total degradation rate
DR_{Tm}	Thermomechanical degradation rate
I_{SC}	Short circuit current
I_{mpp}	Current at the maximum power point
P_{mpp}	Maximum power

T_{max}	Maximum temperature
V_{OC}	Open circuit voltage
V_{mpp}	Voltage at the maximum power point
BIPV	Building Integrated PV
BoM	Bill of material
DHI	Diffuse Horizontal Irradiance
DNI	Direct Normal Irradiance
FEM	Finite Element Method
GHI	Global Horizontal Irradiance
Gpoa	Global plane-of-array irradiation
IDEAS	Integrated District Energy Assessment by Simulation
IGBT	Insulated Gate Bipolar Transistors
MPP	Power at Maximum Power Point
nMAE	normalized mean absolute error
nMBE	normalized mean bias error
nRMSE	normalized root mean square error
OMWB	Opaque multiwire all black
OMWT	Opaque multiwire terracotta
PLR	Performance Loss Rate
RC	Resistor Capacitor
RH	Relative Humidity
S_x	String_(x)number
ST5BB	Semi-transparent 5 busbars
STC	Standard Testing Conditions
STMW	Semi-transparent multiwire
T	Temperature
TMY	Typical meteorological year
UV	Ultraviolet
FF	Fill Factor

Due to their integration, BIPV systems typically function under distinct conditions in comparison to open installation counterparts. The variances in operational conditions could impact PV performance and reliability, with potential positive or negative implications. For example, regarding the operating conditions, the authors in [2] have experimentally shown that BIPV modules installed in a mid-latitude country (Switzerland) with a reduced or restricted rear side ventilation operated at temperatures 20°C–30°C higher than the same modules installed in an open-rack configuration. Comparable research has also demonstrated elevated operating temperatures within insulated BIPV systems in contrast to open rack or ventilated BIPV systems [3], [4], [5], associating these higher temperatures with reduced PV performance or energy output.

In [6], the influence of elevated operating temperatures on the reliability of BIPV modules was investigated. The authors compared two sets of modules with two different mounting configurations (ventilated and insulated). One set of modules showed a significant difference in performance loss rates between ventilated and insulated (i.e., PLR changed from 0.01%/year for ventilated to −0.42%/year for insulated). The other set of modules showed an opposite trend, the detailed explanation is given by Gok et al [6]. The authors in [7] assessed a 20-year pilot BIPV system at Politecnico di Milano to evaluate the performance and reliability of the system. They observed that after 20 years, the system is still performing under warranty limit (i.e., less than 20 % performance loss). However, the system is experiencing multiple degradation/failure modes mainly discoloration of the encapsulant, delamination, chalking of the backsheet, corrosion due to moisture ingress and snail trails. In [8] the authors assessed 55 BIPV systems in Switzerland ranging from 5 – 10 years of field exposure. The authors evaluated a median PLR of only 0.06 %/year. This is a surprisingly stable performance compared to standard PV modules with median degradation rate of 0.5 %/year as reported in other studies [9], [10], [11], [12]. A recent study [13] compared the reliability of different PV configurations using a fleet of PV systems and found comparable median performance loss rates of BIPV systems and ground/open rack systems.

Based on the studies about the reliability of BIPV systems discussed in the previous paragraphs, we cannot infer a clear correlation between elevated operating temperature and PV reliability. Additionally, there is limited spatial and temporal data to make a statistically significant correlation. Indeed, the authors in [8] and [13] mention the spread in the data making it difficult to make any conclusions. The variations in PV bill of material (BoM) components and PV technologies also limit a clear understanding of the reliability issues due to elevated operating temperatures in BIPV systems as. Moreover, the operating conditions or mission profiles of PV modules in BIPV system can vary according to the mounting design, location, and specific project requirements hence affecting the performance and reliability differently [14].

In summary, the performance and reliability of BIPV systems cannot simply be generalized based on only the limited historical data available. Additionally, designing an experiment to mimic all the different aspects that might influence the performance and reliability of BIPV system is almost impossible or simply very expensive in time and costs. A quick shortcut is always to use mathematical models, as this can increase the degree of freedom to simulate different performance and reliability influencing aspects.

This study addresses the existing challenge of the effectiveness of existing PV simulation software in evaluating the performance and reliability of BIPV systems. While some commercial PV performance simulation software packages now have the option to select the mounting features of a BIPV system, most only allow for simple roof mounting selections. Few provide functionalities to simulate / select the rack, gap, flush mounting, roof parallel, roof-integrated rear ventilation, roof-integrated no ventilation and façade integrated [15]. The simplification in the simulation packages limits the exploration of different performance and reliability influencing variables which could be specific to a given BIPV project. Additionally, several frameworks have been proposed to simulate the performance and optimize BIPV systems designs [21], [22], [23], [24], [25]. To our knowledge, none of the available simulation packages and frameworks considers the degradation modelling to simulate the reliability of BIPV modules based on reliability influencing variables. To explore the performance and reliability aspects in a BIPV system a more detailed physics-based approach, that also considers degradation models, is required.

This paper introduces a novel, bottom-up physics-based simulation framework for BIPV systems performance and reliability modelling. The proposed framework is based on different sub-models/simulation frameworks such as the building simulation model/library so-called Integrated District Energy Assessment by Simulation (IDEAS) [19], [21], the patented imec energy yield simulation framework [22], [23] and the physics-based empirical degradation models proposed in our previous studies [24], [25]. Additionally, inverter reliability models are applied to the simulation framework to model the reliability aspects of PV inverters in a BIPV system. The IDEAS library is used to simulate the cavity or the micro-climate temperature around the PV module in a building environment. The energy yield simulation framework is used to simulate the module temperature and the electrical performance. The degradation model uses the module temperature and plane of array irradiance from the energy yield framework together with ambient relative humidity to simulate the degradation rates of PV modules. In this work:

- We use the experimental data from a BIPV demonstrator to validate the different components of the proposed BIPV simulation framework (i.e., cavity, module temperature and electrical models)
- Perform 'what if' simulation of the performance and reliability of a BIPV system in open, ventilated, and unventilated cavity. This is done in three different locations representing three different climate classification: Moderate (Belgium), Hot and dry (Kuwait) and Hot and Humid (Singapore).
- Perform 'what if' simulations of the performance and reliability of a BIPV system in an open and strong shading scenario to evaluate trade-offs of under-performance and prolonged lifetime of continuously shaded BIPV systems.

2. Methodology

This section describes the different modelling components of the proposed performance and reliability simulation framework for a BIPV system: Case study a vertical BIPV installation with ventilated and unventilated cavity.

2.1. General features of BIPV energy yield/reliability modeling framework

The BIPV energy yield/reliability modeling framework is composed of four essential parts, a general diagram with a description of the different inputs is given in Figure 1.

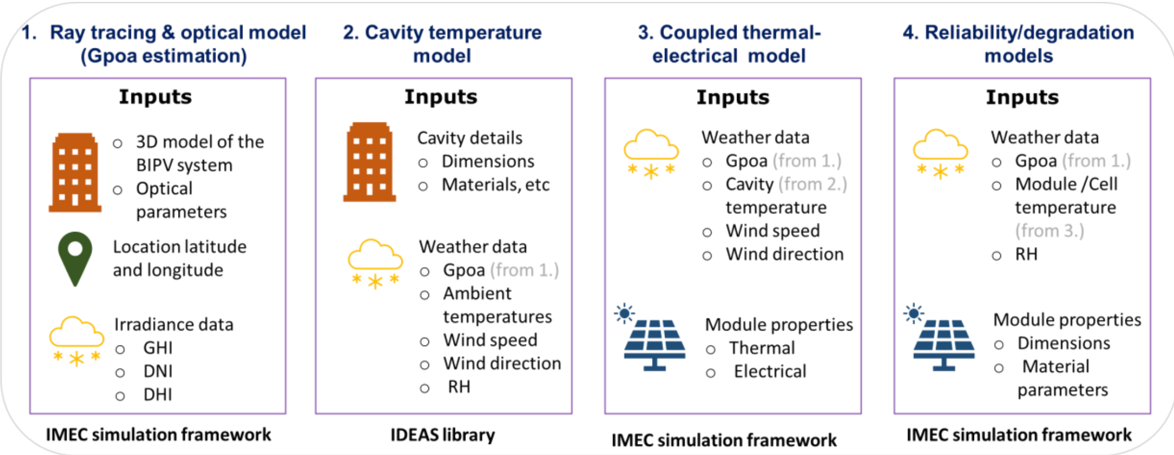

Figure 1. The schematic of BIPV energy yield and reliability modeling framework used in the study.

2.1.1. Ray tracing model (Estimation of plane of array irradiance)

The ray tracing model uses the global horizontal (GHI), diffuse horizontal (DHI) and direct normal (DNI) irradiance data to calculate the global plane-of-array irradiation (Gpoa) on the PV modules. Ray tracing available in the Radiance software package [26], a sophisticated ray tracing model that simulates the path of solar rays as they interact with PV elements. By tracing the trajectory of individual rays through the atmosphere and considering factors such as cloud cover, shading, and atmospheric conditions, the model provides a precise estimation of plane-of-array irradiance (Gpoa) on all PV elements. It also considers interactions with intricate 3D scenes hence it allows to simulate how the different parts of the 3D BIPV system model affect energy generation. Furthermore, the optical model utilizes in-plane irradiance data to calculate the absorption, transmission, and reflection of irradiation energy for every material layer within the photovoltaic module. The optical modeling procedure encompasses the determination of absorption, transmission, and reflection values for the environment, the cover layer (e.g., glass layer) of the photovoltaic module, and the encapsulation layers.

2.1.2. Cavity thermal and airflow models

In a BIPV setup, multiple heat transfer processes occur at different positions and layers. Airflow passing through ventilation openings evacuates hot air from the cavity, thus cooling the module. Conduction, convection, and radiative heat transfers occur within the cavity. As only a proportionally small amount of solar irradiation is converted to electricity by PV cells, most of the energy is lost as heat to the surrounding environment, including the module's cavity, its back wall, and the building interior thermal zone to which it is attached. These heat transfers follow the physical laws of conduction, convection, and radiation. Detailed descriptions of the cavity thermal and airflow models are provided in references [19], [27].

The thermal model for BIPV systems was developed using the IDEAS library [21] of Modelica, which specializes in building simulation. This library allows for the modeling of heat transfer phenomena on building facades, facilitating the integration of the BIPV model as a component of the facade structure. To enhance the thermal performance of the model, additional analytical expressions were incorporated, such as Blocken and Montazeri forced convective heat transfer coefficients at building facades and roofs [28]. These correlations consider various aspects of the built environment, including building dimensions and wind effects.

The airflow model, which is integrated with the thermal model, comprises of two main components: airflow behavior through ventilation openings and airflow within the cavity interior. Airflow through the cavity is calculated as a function of discharge coefficient and pressure difference, implemented through the opening component in the IDEAS library and connected to both the boundary and volume of the cavity. Air movement inside the cavity is primarily influenced by thermal buoyancy, driving natural convection. This is achieved by using the medium column component and connecting it between each vertical BIPV segment. Figure 2 illustrates the airflow pattern and the heat transfer processes with the BIPV cavity.

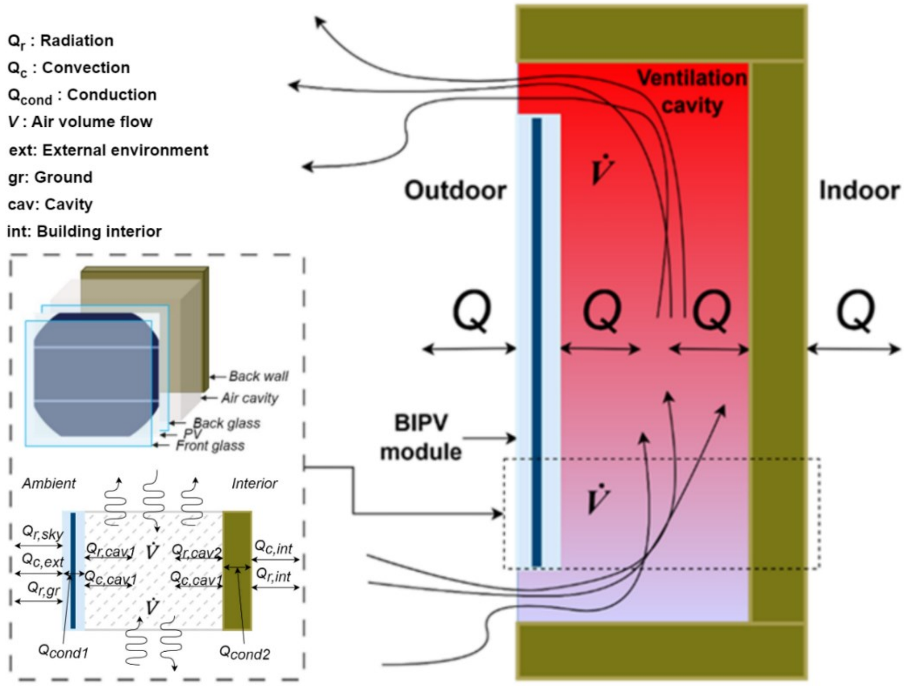

Figure 2. Illustration of the heat transfer and airflow behavior within the BIPV cavity

2.1.3. Coupled thermal-electrical model.

The thermal model used in imec simulation framework is represented by an equivalent resistor-capacitor (RC) circuit where the equivalent thermal resistances and capacitors are computed on each layer of the PV module as described in [22], [23], [29]. A short and clear description of the coupled thermal-electrical model of imec is present in [29] and re-used here for consistency. The thermal model of each PV module component or layer is represented by an RC pair and a current source to consider heat generation within the layer. The model of the layered PV module structure is assembled as a 'Continued fraction circuit' scheme, also called ladder network. Thermal radiation and convective cooling of the module surfaces is modelled by means of input-dependent thermal resistors, which may have time-varying, highly non-linear properties. Solving the circuit enables the computation of heat conduction within the layered structure. This is a crucial element to improve the accuracy of solar cell temperature evaluation.

In the electrical model the single diode equation with a temperature dependent diode, series, and shunt resistances is used. The coupling between the thermal and electrical models is established by considering the net power absorbed in the solar cell (provided by the optical model). Some part of this net power is extracted from the solar cell in the form of electrical power. This is computed from the single diode equation and influenced by the actual operating point. Therefore, the complex dependency of extracted electrical power on fluctuating weather conditions, on non-uniformities causing mismatches (e.g. partial shading) and on electrical operating point is fully represented. The other part of the net power is converted into heat and injected to the thermal network by a current source in the solar cell layer of the thermal RC network. The latter and the above-mentioned heat transfer processes influence the solar cell temperature, which affects the temperature dependent diode, altering the extracted electrical power.

2.1.4. Reliability/degradation models: PV degradation models

To evaluate the non-reversible degradation rate, we applied the model proposed in [24]. The total degradation rate of power (DR_T[%/year]) is estimated as a function of specific degradation mechanisms/processes based on the applied climatic stresses as [24]:

$$DR_T = A_N \cdot (1 + \mathrm{DR_H})(1 + \mathrm{DR_P})(1 + DR_{Tm}) - 1 \qquad \text{Eq. (1)}$$

Where DR_H, DR_P and DR_{Tm} are the degradation rates for hydrolysis, photodegradation, and thermomechanical degradation, respectively. These rates are evaluated as functions of environmental stressors as [24], [30]:

$$\mathrm{DR_H(T, RH)} = \mathrm{A_H} \cdot \exp\left(\frac{-\mathrm{E_{aH}}}{\mathrm{k_B} \cdot \mathrm{T}}\right) \cdot \mathrm{RH^n} \qquad \text{Eq. (2)}$$

$$\mathrm{DR_P(UV, T, RH)} = \mathrm{A_p} \cdot \mathrm{UV^y} \cdot (1 + \mathrm{RH^{n_1}}) \cdot \exp\left(\frac{-\mathrm{E_{aP}}}{\mathrm{k_B} \cdot \mathrm{T}}\right) \qquad \text{Eq. (3)}$$

$$\mathrm{DR_{Tm}(\Delta T, T_{max})} = \mathrm{A_T} \cdot (\Delta\mathrm{T} + 273)^{\mathrm{x}} \cdot \mathrm{C_r} \cdot \exp\left(\frac{-\mathrm{E_{aT}}}{\mathrm{k_B} \cdot \mathrm{T_{max}}}\right) \qquad \text{Eq. (4)}$$

Here , k_B (8.62 × 10^{-5} eV/K) is the Boltzmann constant, T [Kelvin] is the annual average module temperature, T_{max} [Kelvin] is the annual average maximum temperature of the module, ΔT is the annual average cyclic temperature of the module, UV [kWh/m^2] is the total annual UV dose, RH[%] annual average relative humidity, C_r[cycles/year] annual temperature cycling frequency (assumed as I cycle per year). Definition of other model parameters and values used are presented in Table 2 below.

Table 2: Definition of model parameters and values used in degradation rate simulation.

Parameter	Quantity
A_N normalization constant of the physical quantities	$1\ year^{-2}$
A_H exponential coefficient for hydrolysis	$4.91e7\ year^{-1}$
A_P exponential coefficient for photodegradation	$7.3e7\ (kWh/m^2)^{-1}$
A_T - exponential coefficient for thermomechanical degradation	$2.04\ cycle^{-1}$
E_{aH}, E_{aP} and E_{aT} [eV] activation energies, for hydrolysis, photodegradation and thermomechanical degradation respectively	Simulated as a distribution
n, n_1, y and x are model parameters that describe the effect of RH	$n = 1.9, n_1 = 0.1,\ y = 0.63$ and $x = 2.04$

The parameter of the models that can be linked to the PV bill of materials and the most sensitive parameter is the activation energy [25]. Other model parameters are used as they are presented in [24], [25] but since we are simulating a different PV module as those presented in [24], [25], the activation energies (E_{aH}, E_{aP} and E_{aT}) need to be varied. Since we do not have historical degradation data of the specific module under evaluation, we applied a statistical approach by using a population of over 1000 different activation energies to perform a Monte Carlo simulation approach. By using a non-central F distribution continuous random variable generator [31] and applying some boundary conditions of activation energies for each degradation mechanism [24], [25], [32], [33], a distribution like the one in Figure 3 is generated for E_{aH}, E_{aP} and E_{aT}.

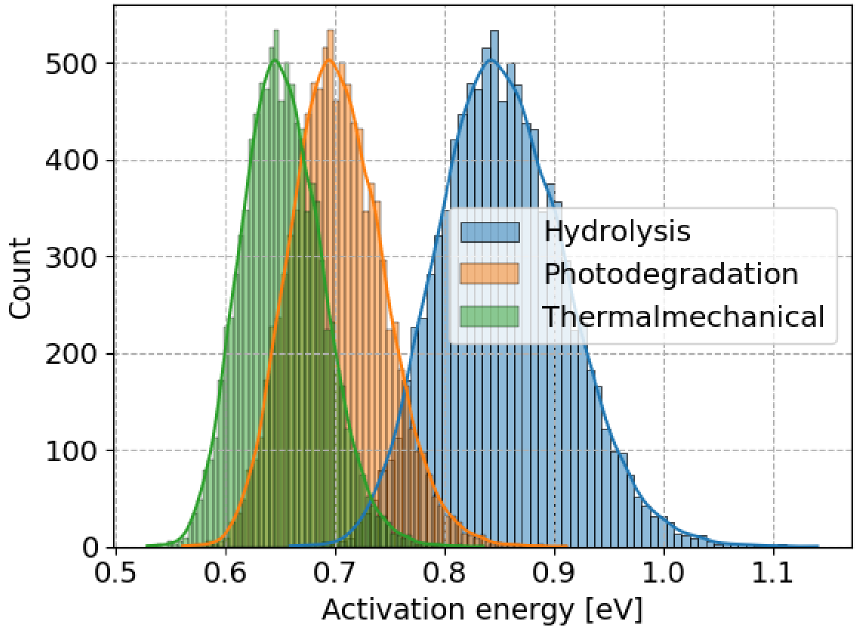

Figure 3. Distribution of activation energies for each degradation mechanism used in the evaluation of the degradation rates.

The study defines the lifetime of the PV modules as the duration until the module's power diminishes by 20% from its initial value at standard testing conditions (STC). This duration is calculated from the total degradation rate (DR_T) under the assumption of linear degradation in Eq. (5). Figure 4 shows the relationship between PV module lifetime and degradation rate using Eq. (5).

$$Lifetime = \frac{0.2}{DR_T} \qquad \text{Eq. (5)}$$

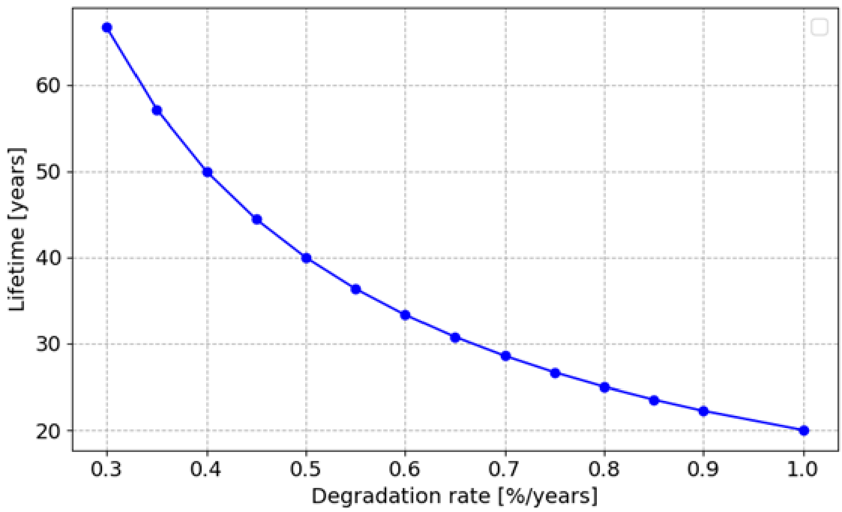

Figure 4. Lifetime Vs degradation rates assuming a linear degradation. Lifetime is defined as 20% loss of the initial power.

2.1.5. Reliability/degradation models: COMSOL Multiphysics PV module thermomechanical stress model

The physics-based empirical models for degradation rate evaluations described in (a) above do not consider the underlying steps leading to the simulated degradation rate. To understand the underlying processes or physics leading to simulated degradation rates, detailed physics-based models/ tools like COMSOL Multiphysics must be used. In this paper, we applied a Finite Element Method (FEM) simulation by COMSOL Multiphysics to investigate the underlying degradation processes due to thermomechanical stress and their correlation with operating temperatures of the PV module.

A PV module is a complex and multilayered structure which includes many elements. For this reason, a thermomechanical simulation incorporating all the parameters of a full PV module is computationally expensive. To simplify the computations, the thermomechanical study is initially conducted on the PV module excluding the ribbons, interconnections, and solder, with COMSOL Multiphysics. Afterwards, for the estimation of the thermomechanical stress on the ribbons, solder and cells, the global-to-local approach is utilized. According to it, a specific part of the full geometry is selected, which includes the ribbons, solder, and interconnection between two cells. The PV module assumed is the one including five-busbar cells (see section 2.3.1). Only half of the PV module was modeled since symmetry conditions were applied, for faster computation. The PV module is attached within a wooden frame by rubber. This type of attachment keeps it in place while providing the capability of limited expansion. For the local approach, the studied geometry belongs to the interconnected cells at the top left corner of the PV module, on the first busbar. The displacement of the glass calculated from the global model was applied as a boundary condition for the local model. All the geometry and meshing details, boundary conditions and material properties are explained in the appendix section B. The boundary conditions selected is a combination of rollers and is preferrable when compared to simple constraints, since it allows a slight movement and expansion in the lateral direction, but it still limits the movement degrees. The selection described is suitable for the simulation of the studied case, due to the installation of the PV module (attachment to wooden frame by rubber). The reference temperature utilized for each stationary thermomechanical simulation was 20 °C, since all the material properties are reported for this specific temperature (literature [34], [35], COMSOL material library). For this reason and due to lack of experimental results, the material properties were assumed constant with temperature.

2.1.6. Reliability/degradation models: Inverter reliability model

The lifetime of PV inverters is greatly impacted by the system's operating conditions and the power production. These conditions, including solar irradiance and ambient temperature, eventually lead to thermomechanical stress on the PV inverter components. Previously, reliability of converters was evaluated through black box models, assuming consistent failure rates [36], [36], [37]. A prominent standard for such evaluations was the American Military Standard MIL217-F [38]. The notable deviation between calculated and observed lifetimes, deduced from field returns, has directed research towards the Design for Reliability (DfR) methodology, that can be incorporated in the design phase of the PV inverter system considering life limiting factors[39], [40].One of the dominant failure mechanisms of IGBT modules in the PV inverter is the bond wire fatigue and solder joint cracking due to temperature excursions [41], [42].

The reliability of power electronic devices can be evaluated by the mission profile-based lifetime estimation technique as part of the design for reliability approach [43]. In this work, a case study of a 3-kW single-phase two-stage grid-connected PV inverter is constructed in Simulink, Matlab. A boost converter and full-bridge DC-AC inverter is employed with a DC link voltage of 400 V. The Insulated Gate Bipolar Transistors (IGBTs) and diodes from a leading manufacturer [44] are utilized and the PV output power from the proposed BIPV simulation framework is used as input to the reliability model of the PV inverter, in the same approach as [45].

The PV module OMWB (Opaque multiwire all black) from the BIPV setup at EnergyVille 2 building in Genk, Belgium is chosen for the simulation. In the simulation, two strings are connected in parallel, and each string consists of 14 modules in series to achieve 3.4-kW rated power (array slightly oversized to account for the power loss due to the vertical inclination). In this study the inverter is assumed to be placed indoors inside the building and the indoor temperature is assumed to be fixed at 25°C. To be able to assess the reliability of the inverter system, the operating conditions, meaning the ambient temperature and the power at maximum power point (MPP), will be translated into thermal loading of the PV inverter. The input power is evaluated for the three scenarios as in the case for the PV module reliability analysis (i.e., open rack, ventilated BIPV and Unventilated BIPV scenarios). Two locations Brussels, Belgium and Kabd, Kuwait, are used in the analysis.

After that, by using lookup tables, the mean junction temperature T_{jm} and the cycle amplitude ΔTj are obtained for the yearly mission profiles of the two locations. Then, a cycle counting algorithm is applied to obtain regular loading ranges. The rainflow cycle counting algorithm is a technique that identifies the thermal cycles in a variable loading history [46]. This algorithm is developed to consider the stress–strain hysteresis loop in temperature loading history, which is the physical basis of this algorithm, each closed hysteresis loop represents a cycle. The junction temperature cycles in the power device have patterns that differ in the cycle amplitude and period. Hence, the rainflow cycle counting algorithm is used to obtain regular loading ranges, from which the thermal loading parameters: mean junction temperature T_{jm}, the cycle amplitude ΔT_j, the cycle period t_{on}, and the number of cycles n_i for each regular loading i can be determined. These parameters are then applied to the lifetime model in [47] to find the number of cycles to failure (N_f). Finally, the lifetime consumption (LC) for one year is obtained and the Monte Carlo simulation and reliability assessment are performed considering the uncertainties and variation in the lifetime model parameters [48].

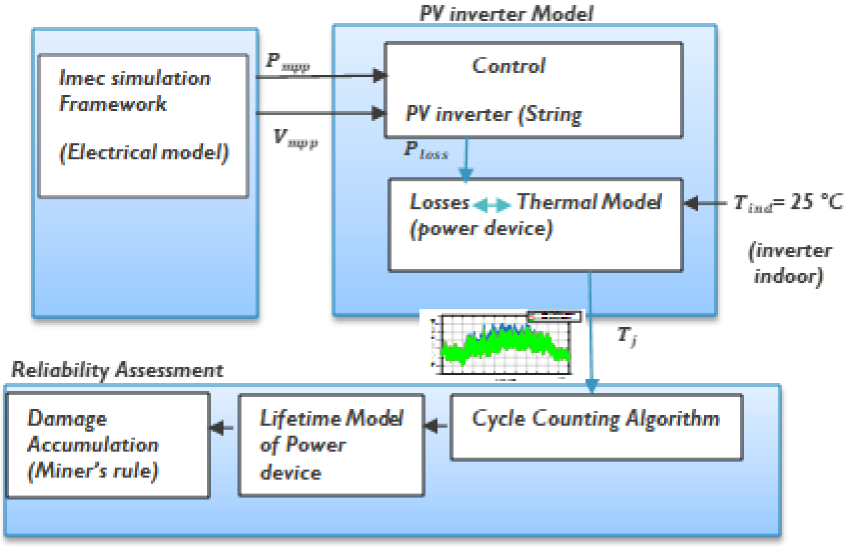

Figure 5. Mission Profile-based lifetime Estimation methodology using proposed BIPV simulation framework. P_{mpp} is the power at maximum power point, P_{loss} is the power loss dissipated in the power devices and T_{ind} is the indoor temperature.

2.2. Description of the “what-if” scenarios

2.2.1. BIPV installation design scenario: Effect on PV module and inverter reliability

To demonstrate the effect of BIPV installation design on the performance and reliability of the PV modules and inverters, three scenarios are considered: Open rack (used as reference), ventilated BIPV representing a BIPV installation with open air cavity and unventilated BIPV representing a PV installation with closed air cavity as shown in Figure 6. For all three scenarios, the same module (OMWB in Table 3) is simulated facing south and vertical (90° tilt angle).

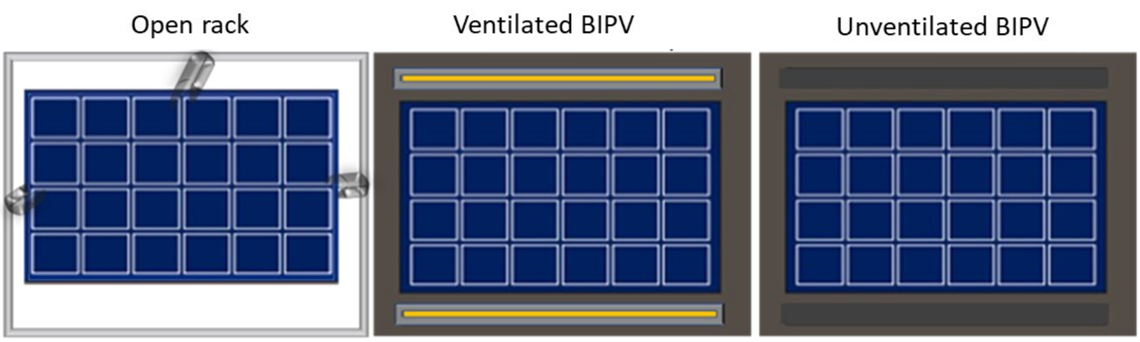

Figure 6 Simulation scenarios; Open rack, ventilated BIPV and Unventilated BIPV.

2.2.2. Shading scenarios: Effect on energy yield and PV degradation

There are countless shading scenarios that a BIPV system could experience and simulating all the different scenarios is not the scope of this study. In this study, we simply assess if there would be some lifetime benefits due to continuous shading effect of a BIPV system in a building environment. A PV module operating under continuous shading is expected on average to experience less stress factors such as irradiation and operating module temperature compared to unshaded systems.

To assess the impact of shading on PV performance and reliability, we assumed two extreme scenarios; i) a BIPV system without any surrounding shading object and ii) a BIPV system surrounded by two tall (12-meter tall) buildings as shown in the SketchUp model in Figure 7. For the simulation, the OMWB module described in Table 3 was used. Two bypass diodes are added to the module to have a more realistic shading tolerance situation. The building facade is composed of 8 rows (strings) of modules, each containing 11 modules. The modules in each row are connected in series and connected to a maximum power point tracking (MPPT) in the simulation. The proposed BIPV simulation framework is used to simulate the cavity temperature, energy yield and degradation of the entire PV system on the facade. This analysis is conducted for two distinct locations: Genk, Belgium and Kabd, Kuwait, utilizing typical meteorological year (TMY) data. The simulation is performed assuming a ventilated BIPV system installation. The proposed framework could be applied to simulate different shading scenarios e.g dynamic shading events or including future vegetation growth or urban development that might add more shading on the BIPV system.

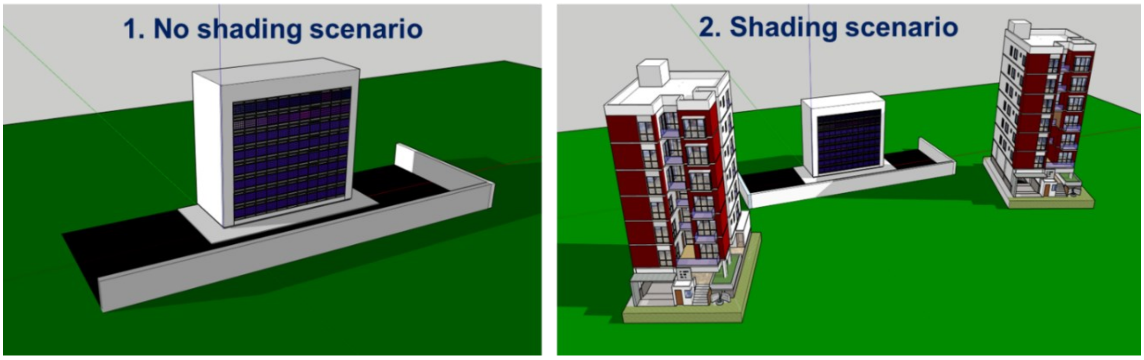

Figure 7. Simulated No Shading (1) and shading (2) scenarios.

2.3. Data used in this study.

2.3.1. Experimental data

At the rooftop of EnergyVille 2 building in Genk, Belgium, different BIPV experiments are being performed for different purposes (see Figure 8). Useful for this study are the four modules highlighted with a green boundary. All modules are glass-glass modules, the differences and details of the modules are described in Table 3.

Figure 8. BIPV facade experimental setup at EnergyVille 2 building in Genk. In 1, the modules highlighted with a green boundary are the ones investigated. In the middle (2) shows the inside of the building and (3) shows the south and east view of the building. The modules investigated here are in the south (S) facade.

Table 3. Description of module properties

Module 1	Module 2	Module 3	Module 4
Name: OMWT 4X6 cells, Opaque multiwire terracotta <u>Electrical</u> Isc : 7.116 A, Voc : 17.424 V, FF: 80.9%, Pmpp: 100.3 W <u>Installation</u> Open cavity	Name: OMWB 4X6 cells, Opaque multiwire all black <u>Electrical</u> Isc : 8.551 A, Voc : 17.552 V, FF: 80.5%, Pmpp: 120.8 W <u>Installation</u> Open cavity	Name: STMW 4X4 cells, semi-transparent multiwire <u>Electrical</u> Isc : 9.100 A, Voc : 11.724 V, FF: 77.1%, Pmpp: 82.3 W <u>Installation</u> Closed cavity	Name: ST5BB 4X4 cells, semi-transparent 5 busbars <u>Electrical</u> Isc : 9.460A, Voc : 10.939 V, FF: 76.7%, Pmpp: 79.4 W <u>Installation</u> Closed cavity

Different temperature and relative humidity sensors are installed at different places around the modules. The sampling rate for both temperature and relative humidity sensors is 1 minute. Additionally, I-V curves measurements are done on a minutely resolution and a pyranometer is installed in the same plane as the modules to measure the in-plane irradiance. Other weather data such as the wind speed, ambient temperature and ambient relative humidity are also measured at the weather station on the EnergyVille 1 building just a few meters from the BIPV setup. Data has been collected for a period of one year from 02/06/2022 to 31/08/2023.

2.3.2. TMY data

For shading scenarios and long-term performance and degradation evaluation, typical meteorological year (TMY) data downloaded from PVGIS [49] was used. We selected data from four locations representing three different climate zones: moderate climate (Brussels and Genk, Belgium) and hot and dry (Kabd, Kuwait) and hot and humid (Singapore). In each location, weather data; ambient temperature, relative humidity, wind speed and irradiance required for energy yield and degradation modelling are extracted.

2.4. Statistical analysis

To evaluate the uncertainty in prediction, the normalized root mean square error (nRMSE) Eq. (6), normalized mean absolute error (nMAE) Eq. (7) and the normalized mean bias error (nMBE) Eq. (8) are used. The nMBE metric captures the average bias in the prediction (i.e, to check whether the predictions are overestimated or underestimated).

$$\mathrm{nRMSE} = 100 \cdot \frac{\sqrt{\frac{\sum_{j=1}^{N}(p_j - m_j)^2}{N}}}{\Omega} \qquad \text{Eq. (6)}$$

$$\Omega = \begin{cases} \overline{m}, & \overline{m} \neq 0 \\ m_{max} - m_{min}, & \overline{m} = 0 \end{cases}$$

$$\mathrm{nMBE} = 100 \cdot \frac{\frac{1}{N}\sum_{j=1}^{N}(p_j - m_j)}{\overline{m}} \qquad \text{Eq. (7)}$$

$$\mathrm{nMAE} = 100 \cdot \frac{\frac{1}{N}\sum_{j=1}^{N}|p_j - m_j|}{\overline{m}} \qquad \text{Eq. (8)}$$

Where p is the predicted data, m measured data, $\overline{m}$ is the mean of the measured data, m_{max} and m_{min} the maximum and minimum values of the measured data respectively.

To evaluate the losses due to shading of a variable x ($\mathrm{Var_x}$) with x being irradiance or energy yield, we use:

$$\text{Shading loss Var}_x = 1 - \frac{Var_x\ No\ shading}{Var_x\ Shading} \quad \text{Eq. (9)}$$

3. Results and discussion

3.1. Assessing the temperature differences in BIPV modules installed with open and closed cavities

The measured cavity and module temperature around/of the four modules is shown in Figure 9 A and B respectively. From A, depending on the month of the year, the difference between open and cavity temperature can be over 15 °C. The modules with closed cavities operate at higher temperatures than the modules with open cavities as shown in Figure 9B. Even though the modules are not with similar BoM, the observed difference in modules temperature is too big to be linked to differences in BoM. For example, we observed some differences (up to 2 °C) in the module temperature between OMWT and OMWB modules. Since both modules are operating in similar conditions (open cavity), the measured differences can only be related to the differences in the modules BoM, Therefore, we can conclude that the differences in module temperatures between modules in open and closed cavities are due to the differences in cavity temperatures.

Additionally, it's worth noting that OMWT and OMWB modules are mostly identical (multiwire-interconnected cells, UV-blocking encapsulant and backside glass with black coating). The modules differ in the front glass, which is clear for the OMWB module and has a "magenta 5%" coating on the inside for the OMWT module. Although, it's not the scope of this study, it is interesting to observe that small changes in BoM could affect the operating conditions of the PV modules. These differences might have positive or negative impact on the performance and reliability of the PV modules. This is even more relevant for BIPV systems where aesthetics meets energy generation! Further studies will be to simulate the reliability of colored BIPV modules on the long-term performance and reliability in different climate zones.

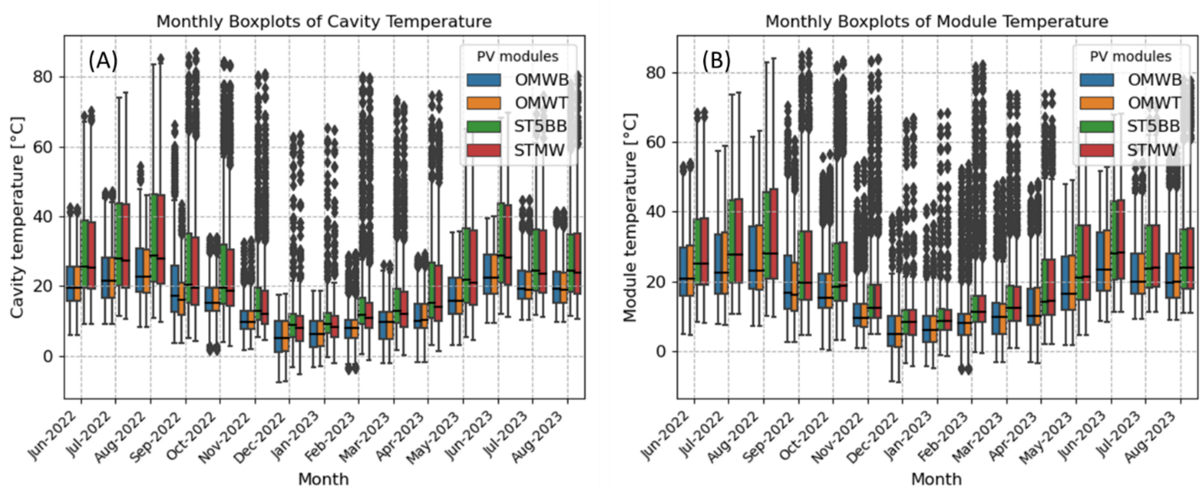

Figure 9. Monthly boxplots of cavity temperature (A) and module temperature (B) for the four modules from June 2022 to August 2023.

3.2. Validation of cavity, module, and electrical models with measured data

Data from the BIPV experimental setup was used to validate the cavity temperature, module temperature and electrical models. We selected data measured during July 2022 because it represented complete and clean dataset for all the required input variables for models' validation process. The validation process was also done using cavity temperature, module temperature and power data from the OMWB module.

Figure 10 shows the scatter plots of simulated Vs measured cavity temperature (A), module temperature (B and D) and power (C). The cavity temperature model shows good predictions at lower temperatures and deviates at higher temperatures as shown in Figure 10A. This is because high cavity temperatures are mostly associated with elevated levels of irradiance, these levels could cause the thermal model to overestimate the cavity temperature.

Figure 10B and Figure 10D show the simulated module temperatures using cavity temperature and ambient temperature as inputs respectively. It is visible that when one neglects the cavity temperature during the simulation and uses the ambient temperature, the module temperature is significantly under-predicted. The under-prediction is obviously related to the lower ambient temperature compared to the cavity temperature (micro-climate conditions) around the module as shown in Figure 11. The difference between ambient and cavity temperature can go up to 14°C as shown in Figure 11B and even more depending on the period of the year.

Additionally, from Table 4 we see that using the ambient temperature instead of the cavity temperature in the electrical model leads to over estimation of the power (indicated by a negative mean bias error) and increases the nRMSE. The conclusion we can make from this analysis is that, when modelling BIPV systems, it is important to first estimate the micro-climate surrounding the BIPV system and integrate them in the electrical / energy yield model instead of directly using the ambient climate conditions. By doing this the prediction accuracy is improved.

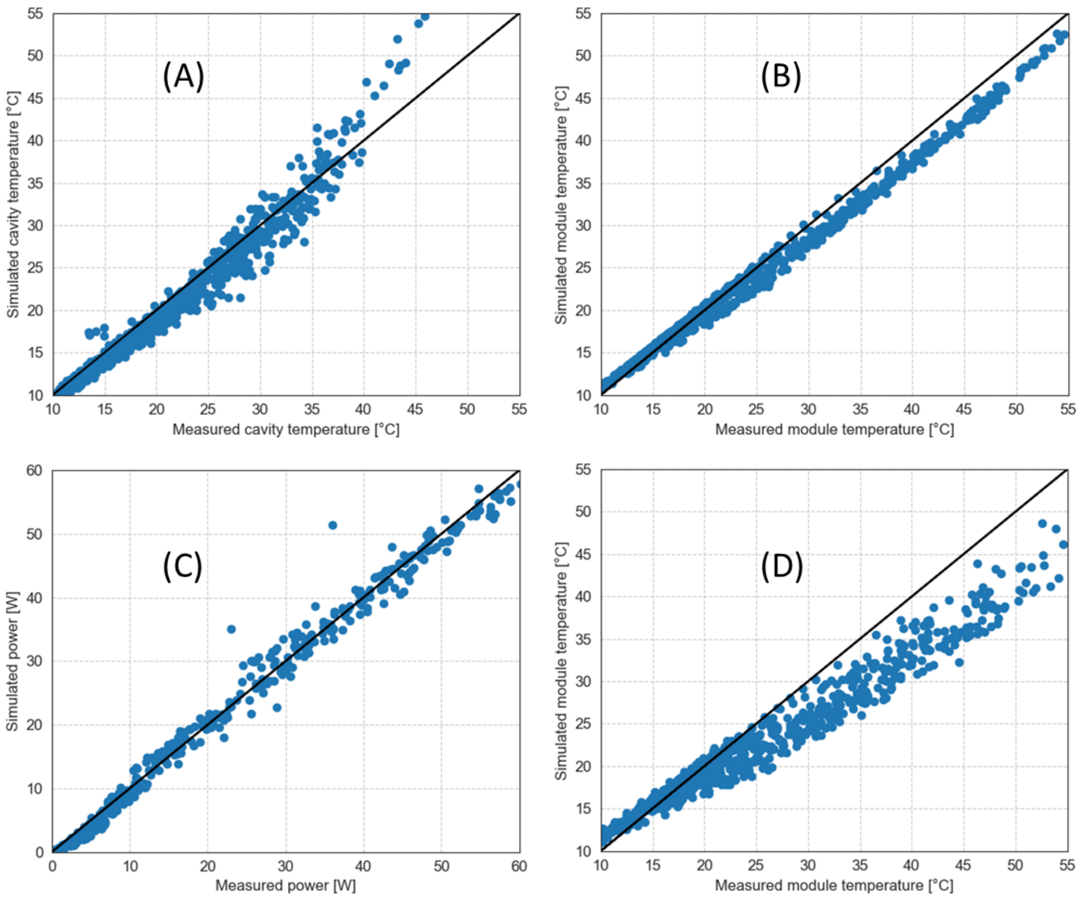

Figure 10 Scatter plots showing simulated cavity temperature Vs measured cavity temperature (A), simulated module temperature Vs measured module temperature (B, D) and simulated power Vs measured power (C). The simulated module temperature in B is done using cavity temperature and in D is done using ambient temperature.

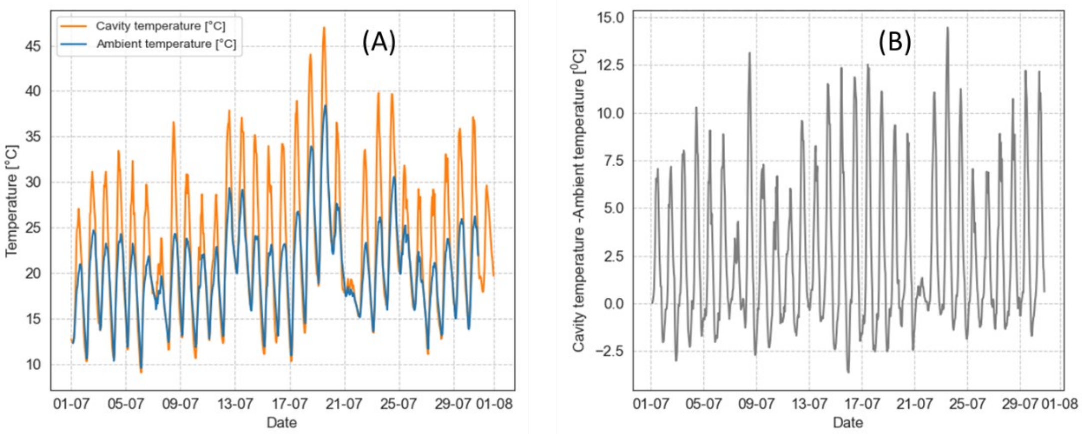

Figure 11. (A) measured ambient (in blue) and cavity (in orange) temperatures and (B) the difference between cavity and ambient temperature.

Table 4. Evaluated error metrics for different models. Module temperature model -Tcav refers to simulated module temperature using cavity temperature as input. Module temperature model -Tamb refers to simulated module temperature using ambient temperature as input. The same applies to the electrical model.

Model // Error metric	nRMSE [%]	nMAE [%]	nMBE [%]
Cavity temperature model	16.81	6.46	3.61
Module temperature model-Tcav	10.02	5.02	3.33
Module temperature model-Tamb	73.71	12.27	10.36
Electrical model - Tcav	15.45	6.12	1.37
Electrical model – Tamb	16.79	5.92	-2.39

3.3. “**What-if**” scenario: Effect of BIPV installation on PV module and inverter reliability

A similar BIPV module (OMWB) is assumed to be installed in three locations Brussels, Belgium (moderate climate), Kabd, Kuwait (Hot and dry climate) and Singapore (Hot and humid climate). The installation scenarios are simulated; open rack, ventilated (open cavity) and unventilated (closed cavity). The proposed BIPV simulation framework is applied to simulate first the micro-climate conditions (cavity temperatures) and the module temperature. And second the effect on PV performance and reliability. Additionally, the effect on the reliability of PV inverters was assessed for two locations (Brussels and Kuwait).

3.3.1. Effect on PV module performance and reliability

The simulated module temperatures using ambient temperature, ventilated cavity temperature and unventilated cavity temperature in the three locations are shown as monthly boxplots in Figure 12. As expected, the module operates at higher temperatures with an unventilated cavity compared to open and ventilated cavity scenario which is consistent with the measurements. The variation in operating temperatures differs from location to location. For example, the simulated module temperature using ventilated and unventilated cavity temperature in Brussels, Belgium Figure 12A did not show a significant difference. On the contrary, for Kuwait (Figure 12B) and Singapore (Figure 12C) we see a significant difference between the simulated module temperature with ventilation and without ventilation.

In Table 5 a summary of the annual mean temperature, the annual maximum temperature and other variables are presented. When comparing the ventilated to unventilated scenarios across the different locations, the annual mean temperature increases by ~1.0 °C and the maximum temperature increased by ~6.0 °C in Belgium. In Kuwait the mean and maximum temperature increase by ~11.0 °C and ~25.5 °C respectively and in Singapore the mean and maximum temperature changed by ~7.7 °C and ~28.8 °C respectively.

The corresponding impact of these variations in module temperatures to the PV module degradation rates and energy yield are shown in Figure 13 and Figure 15 respectively. Overall, the trend remains consistent across all locations, indicating that higher operating temperatures in unventilated conditions contribute to accelerated degradation rates of PV modules, with particularly pronounced effects in hot and dry as well as hot and humid climates.

Comparing the degradation rates for specific degradation mechanisms across the locations and considering only the open and ventilated scenarios, higher degradation rates due to thermomechanical mechanisms are predicted in Belgium and Kuwait compared to Singapore. On the contrary, higher degradation rates due to hydrolysis are predicted in Singapore in comparison to Belgium and Kuwait. The higher thermomechanical degradation rates in Belgium and Kuwait are related to the high temperature variations (ΔT see Table 5) in these regions in comparison to Singapore. The higher relative humidity with high module temperature in Singapore explains the high degradation rates due to hydrolysis compared to Belgium and Kuwait.

When considering the unventilated scenario, the trend changes as we see a higher degradation rate due to thermomechanical mechanisms in Singapore and Kuwait. This is because of the elevated maximum temperatures in some periods of the year which also increases the annual temperature cycles (ΔT see Table 5).

We used COMSOL Multiphysics to further investigate the underlying degradation mechanism of thermomechanical stress to the degradation of the PV module and its correlation with operating temperatures. To do this, different regions of the cells and solder were studied within the local approach, including the center of the cells, the edge of the cells at the region where an interconnection was applied, and the solder at the same region (see appendix B, for the exact location of the studied regions). It must be noted that the results are valid for material properties which do not vary over the range of temperatures (e.g. Young's modulus, thermal expansion coefficient) and could be slightly different in reality, since these values may vary with temperature. However, the results are representative of the behavior of the module components (relative comparison) regarding their state (tension/compression) with temperature increase or decrease.

The results in Figure 14A indicate that the center of the cell experiences both compression and tension, with compression being slightly higher for temperature decrease (when compared to the reference i.e., 20 °C), as the absolute value of the third principal stress (~$3 \cdot 10^7$ N/m^2) is higher than that of the first principal stress (~$2.6 \cdot 10^7$ N/m^2) at -20 °C. The opposite occurs for temperature increase, since the absolute first principal stress (~$4.5 \cdot 10^7$ N/m^2) is higher than the absolute third principal stress (~$4 \cdot 10^7$ N/m^2). The outcome is a result of combined stresses which originate from the thermal expansion of different materials (e.g. combination of the cell, solder, and ribbon), which can further cause cell bending and displacement (appendix B).

Regarding the cell edge and solder Figure 14 and Figure 14C respectively, they undergo more severe tension for lower temperatures and elevated compression at higher temperatures. The reason is that for temperature increase, the attached interconnection moves towards the side of the cell where the respective ribbon is soldered. This movement does not cause significant tensile stress increase to the cell edge and solder, but more compressive stress (appendix B). On the contrary, when the temperature is decreased, compared to the reference, the buckling effect occurs in the opposite direction, moving the cell towards the ribbon which does not contribute to the interconnection. This movement causes more severe tensile stress to the interconnection and the solder attached to it, followed by the cell edge (appendix B).

Figure 14D demonstrates the trend of the von Mises stress for the cell's center, edge, and solder. The von Mises stress is utilized, as it combines both tensile and compressive stress. The highest stress is experienced by the solder, followed by the center of the cell and then the edge. This result could explain that the evaluated degradation rate due to thermomechanical stress / mechanism are mainly related to solder bond failure and increase with increasing temperatures.

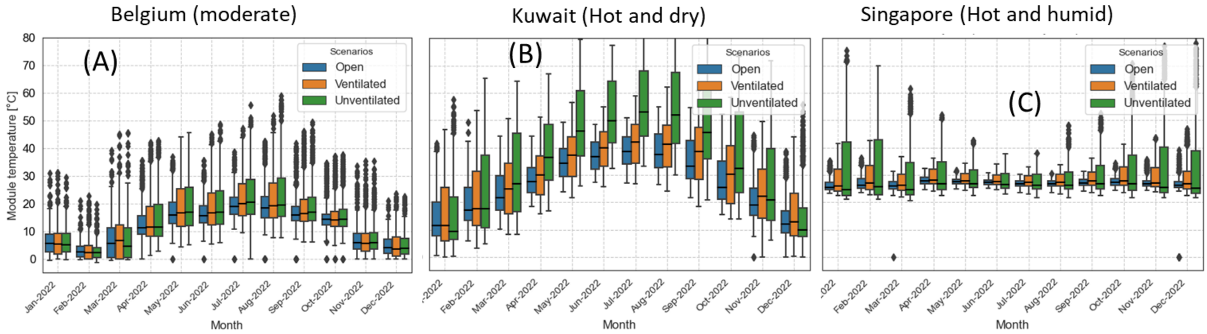

Figure 12. Monthly boxplots of simulated module temperature for open, ventilated, and Unventilated BIPV module in Belgium (A), Kuwait (B) and Singapore (C) respectively.

Table 5. Summary of the annual mean temperature (T), annual maximum temperature temperature (T_{max}), annual mean relative humidity (RH) and UV dose in the three locations. These are the input variables used to simulate the annual degradation rate. T_{max} is evaluated as the 98th percentile or T_{98}. The UV dose is approximated as the 5 % of the plane of array irradiance.

	T [$°C$]	T_{max} [$°C$]	ΔT [$°C$]	RH [%]	$UV\ [kWh.m^{-2} \cdot yr^{-1}]$
Belgium (moderate climate) variables					
Open	18.29	37.55	35.75	79.55	40.62
Ventilated	21.77	40.57	42.76	79.55	40.62
Unventilated	22.04	46.42	45.52	79.55	40.62
Kuwait (hot and dry climate) variables					
Open	35.59	50.77	38.21	29.40	59.74
Ventilated	40.06	56.35	39.74	29.40	59.74
Unventilated	51.15	76.86	67.62	29.40	59.74
Singapore (hot and humid climate) variables					
Open	28.94	33.98	7.75	84.52	25.62
Ventilated	32.67	41.75	14.08	84.52	25.62
Unventilated	40.4	70.5	42.93	84.52	25.62

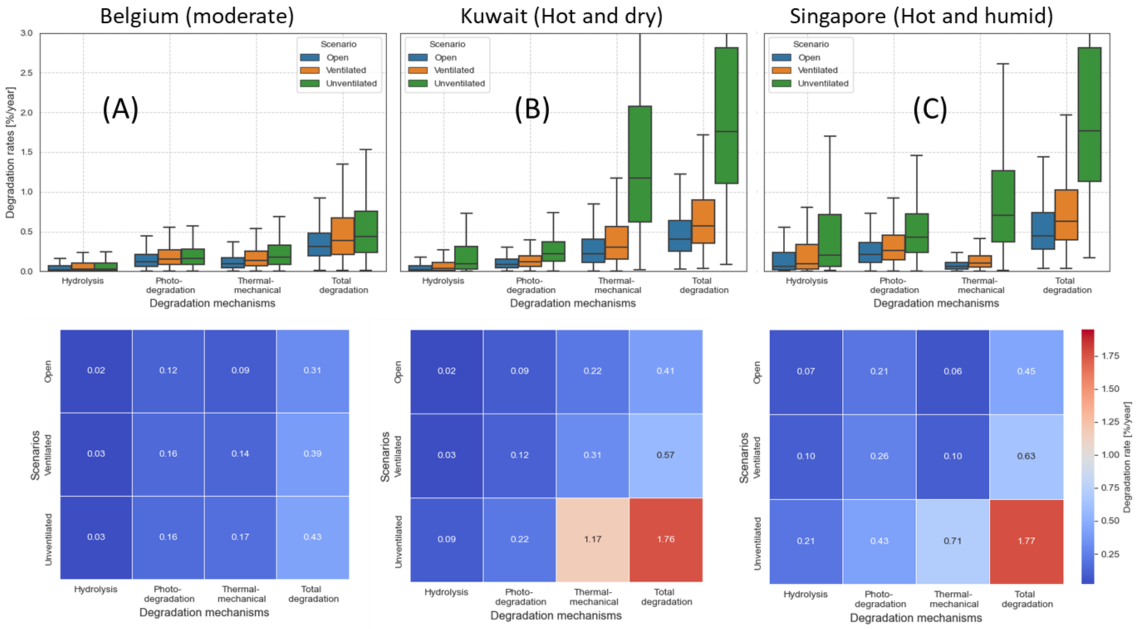

Figure 13. Simulated degradation rates due to the different mechanisms and the combined total degradation for the three scenarios and in the different locations. The heat maps below correspond to the medium degradation rate of each scenario and location respectively.

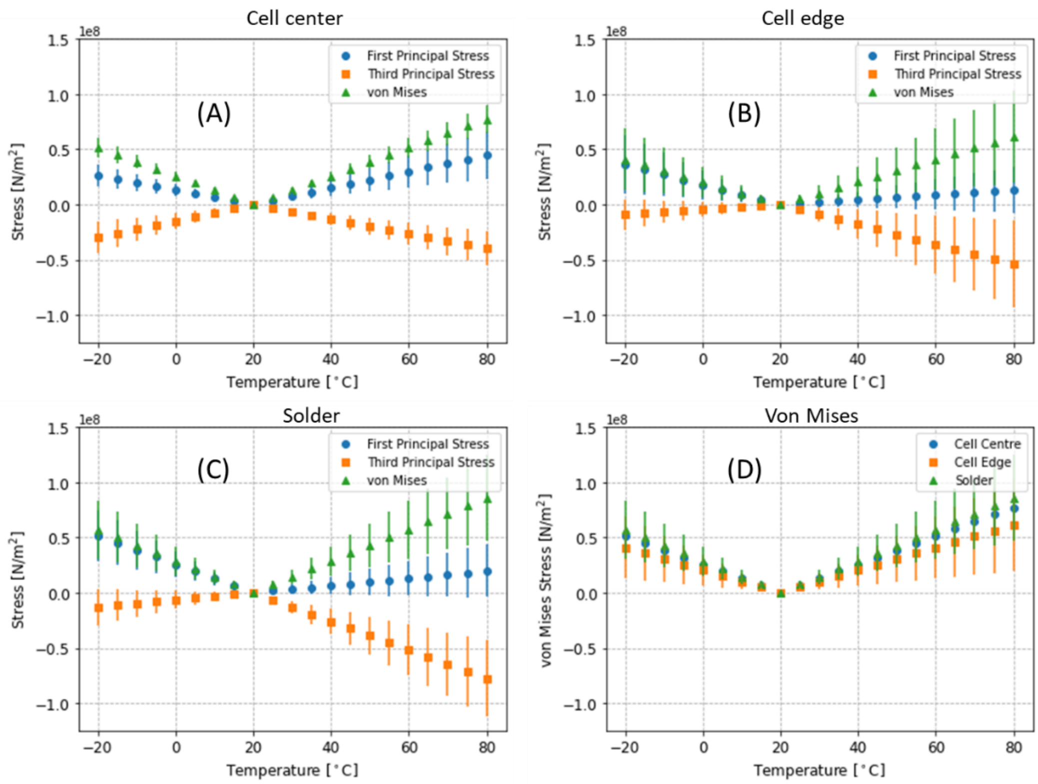

Figure 14. Simulated thermomechanical first principal, third principal and von Mises stresses at the cell center (A), cell edge (B), and solder (C) at different temperatures. Comparison between the von Mises stress at cell center, cell edge and solder at different temperatures (D).

We further estimated the PV module lifetime for the different installation scenarios on the lifetime energy yield. Figure 15A shows the estimated lifetime using the median of the total degradation rate (see heatmaps in Figure 15), the energy yield during the first year of operation without considering degradation and the energy yield evaluated during the module lifetime considering the degradation It is visible that the PV lifetime is reduced significantly in all the three locations when comparing the open scenarios with the ventilated and unventilated scenarios. One observation is that with a proper installation design (i.e BIPV with a ventilated cavity), the lifetime of the modules is still within the 25 – 30 years performance warranty despite operating at higher temperatures compared to standard installation. This is consistent with what some authors have observed in the field data [7], [8]. One explanation to this could be that the modules in a vertical installation receive less UV dose on average compared to standard PV installation at optimal angles (see Figure A 1 in the Appendix). Hence the combined degradation effect of elevated temperatures and UV is reduced.

In Figure 15B the effect of elevated operating temperatures for a BIPV module is visible when comparing the open scenario with the ventilated and unventilated scenarios. The generated energy reduces with increasing operating temperatures. The effect on performance is even stronger when considering the lifetime energy yield with degradation as shown in Figure 15C.

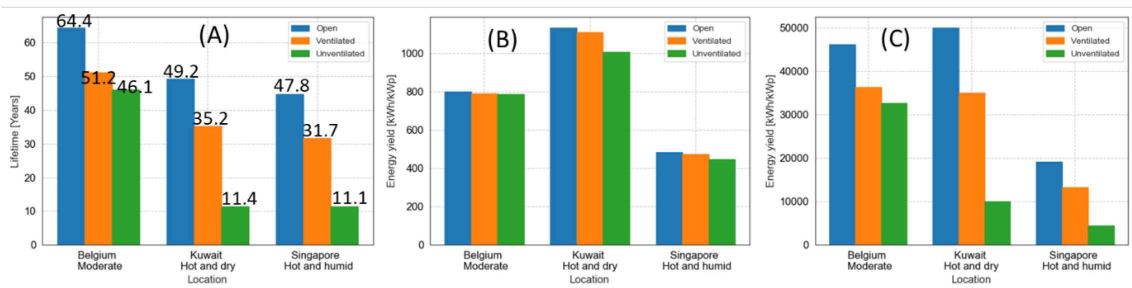

Figure 15. Simulated PV module lifetime (A), energy yield during the first year (B) and energy yield during the lifetime (C) for all the three scenarios and in the three locations respectively.

3.3.2. Effect on inverter reliability

The unreliability function for the IGBT device in system-level (4 IGBTs for full-bridge inverter topology) is carried out for the different configurations in Belgium and Kuwait locations and shown in Figure 16. To have a benchmark with energy production, the annual energy yield together with variations in B10 lifetime, representing the point where 10% of power devices in the population fail, are computed. The open-rack case is taken as a reference and results are shown in Table 5.

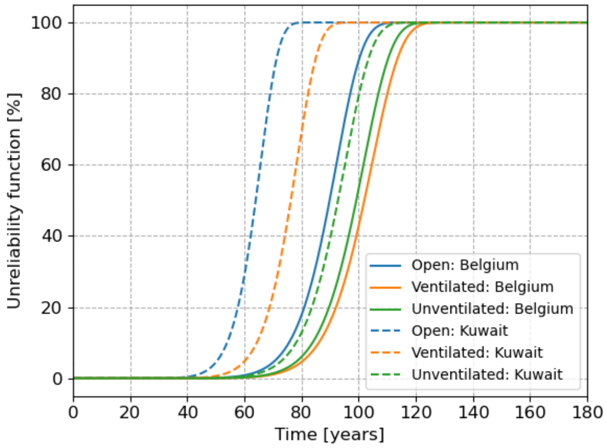

Figure 16. Inverter unreliability function for the three scenarios: Open, Ventilated and Unventilated for Belgium and Kuwait

Table 6. PV Energy yield and increase in B10 lifetime of the string inverter installed in Belgium and Kuwait for different PV plant configurations.

	Energy Yield [MWh/year]	Difference in B10 Lifetime
Belgium (moderate climate)		
Open	2.71	Ref
Ventilated	2.68	+14%
Unventilated	2.67	+11%
Kuwait (hot and dry climate)		
Open	3.84	Ref
Ventilated	3.76	+19%
Unventilated	3.41	+45%

In Belgium, our findings reveal marginal energy production decreases of 1% and 2% for BIPV ventilated and unventilated setups, respectively, compared to the open-rack setup. In Kuwait, a reduction of 2% is observed for the ventilated case and 11% for the unventilated setup, which is due to elevated module temperatures in Kuwait without ventilation. Moreover, the ventilated BIPV configuration extends B10 lifetime for the PV inverter, with a 14% increase in Belgium and a notable 19% increase in Kuwait. This extension is attributed to reduced power output caused by elevated module temperatures. The resulting increase in B10 lifetime translates to lower maintenance costs and reduced replacement frequency, which are crucial considerations in the BIPV context. Notably, the unventilated BIPV case in Kuwait demonstrates an even higher B10 lifetime, marking a 45% increase compared to the open-rack configuration. In contrast, in Belgium, the lifetime is slightly lower than that of the ventilated case, potentially influenced by similar temperatures in both configurations. It is essential to acknowledge that in Monte Carlo simulations, the different lifetime model parameters are modeled as normal distribution with 5% parameter variation, which may account for the observed B10 values.

It is worth noting that the thermal model in this study lacks incorporation of the dynamic and transient thermal response of the IGBT devices. Recognizing this limitation, we emphasize the need to enhance the thermal model in future research. Moreover, the current method for assessing the lifetime of PV inverters face limitations due to inaccurate precision in extracting junction temperature profiles. Consequently, the obtained B10 lifetimes are overestimated, compared to the service lifetime in the field. Additionally, the reliability estimation of PV inverters only accounts for the wear-out failure mechanism, such as bond wire fatigue and solder joint cracking, and the lifetime models for the power devices utilized in these inverters are derived from existing literature, primarily based on power cycling for the designed inverter. This reliance on the same lifetime model may yield unrealistic results. Nevertheless, this lifetime estimation method plays a crucial role in identifying relative differences in B10 lifetime when changing the operating conditions of the system (mission profiles).

3.4. "**What-if**" scenario: Effect of Shading on PV performance and reliability

Figure 17 shows the heatmaps of the annual irradiation for a no shading and shading scenarios in Belgium and Kuwait. The effect of shading is visible in general, and it can also be seen that even in a no shading scenario, there are still shading effects as seen for string S1 to string S8. The location effect is also seen when looking at the shading pattern in Kuwait where string S8 receives less shading from the surrounding buildings compared to other strings. In Figure 18 the losses in irradiance (A) and energy yield (B) due to shading are plotted as percentages for the 8 strings. It is visible that the shading scenario applied in this study has a more impact in Belgium compared to Kuwait. Additionally, as visualized in the heatmaps in Figure 17, shading losses vary across the strings with more shading on string S6 compared to other strings. The irradiance losses are up to ~13 % and ~ 12 % for a BIPV system installed in Belgium and Kuwait respectively. The respective energy losses are up to ~17.5 % and 15.5 % for Belgium and Kuwait respectively. We evaluated the effect on module operating temperatures and the average annual temperature difference between a shaded and unshaded system was ~1.5°C and 1.2 °C in Belgium and Kuwait respectively.

The respective impact of irradiation and temperature variations due to shading on the PV degradation rate, lifetime and performance are shown in Figure 19 and Figure 20. Figure 19 illustrates that the variance in total degradation rates between scenarios with and without shading is 0.02 %/ year for Genk and 0.01 %/year for Kuwait. Figure 20A demonstrates the disparity in lifetime resulting from the change in degradation rates between scenarios with and without shading. Specifically, in Belgium, continuous shading improved the lifetime by approximately 3 years compared to a BIPV system without shading, whereas in Kuwait, the difference was less than 1 year. These variations are consistent with the relationship depicted in Figure 4 between lifetime and degradation rate curve, indicating that minor changes in degradation rates have a significant impact on lifetime, especially at lower degradation rates. It is worth noting that the evaluation was carried out on string S6 with significant shading impact. Generally, the variation in irradiation and temperature showed negligible effect on the degradation rate and the lifetime of the PV module. The effect could also depend on the shading patterns as evident for lifetime extension in Belgium and Kuwait. The extended lifetime, however, could not recover the energy losses due to shading but it reduced the general lifetime shading loss percentage compared to the loss evaluated during the first year (i.e., from -34.82 % in Figure 20B to -28.87 % in Figure 20C). What is noticeable is that the simulated degradation rate on a system level is higher than that on the module level in Kuwait. On assessing of what could be the reason for this, we noticed that the main difference is on the maximum temperature and ΔT. On module level simulation T_{max} = 56.35 °C and ΔT = 39.74 °C and on system level simulation T_{max} = 61.42 °C and ΔT = 49.62 °C. Other variables such as the average module temperature and UV dose are relatively lower for system level simulation compared to module level simulation. Moreover, as demonstrated in [25]], it was revealed that alterations in T_{max} exhibit a greater sensitivity towards degradation rate compared to UV dose. We expect that the difference in T_{max} and ΔT are due to the mismatches due to shading causing some modules to operate at higher temperatures. Although it was not intentional, such mismatches are expected for BIPV systems and could indeed have an impact on the reliability of the PV modules.

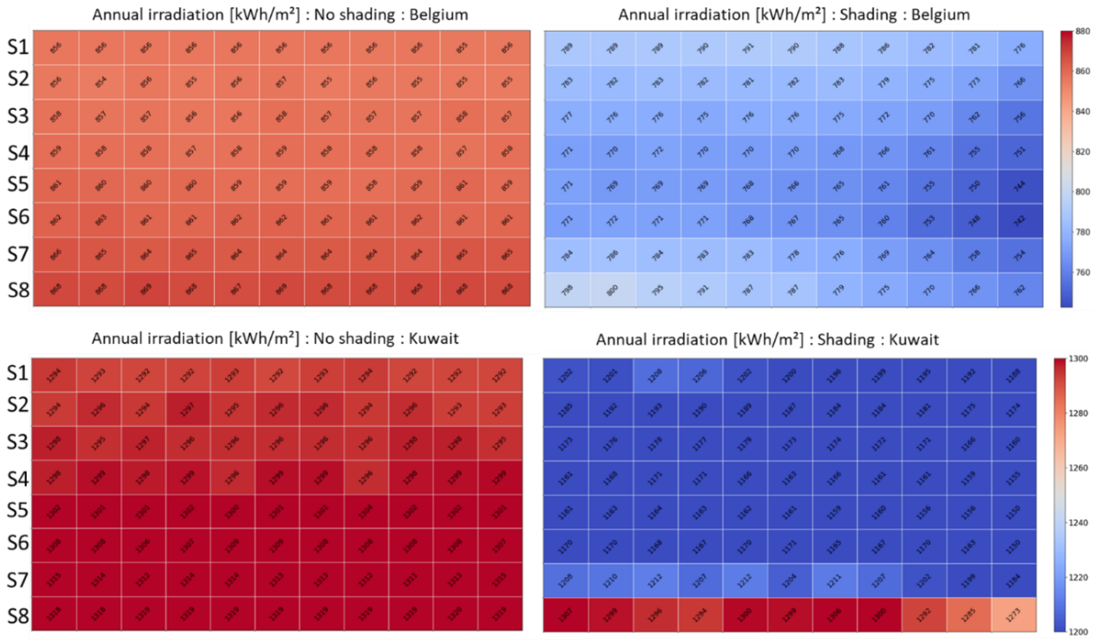

Figure 17. Heatmap of annual irradiation for No shading and shading scenarios in Belgium and Kuwait respectively. S1 – S8 represents the strings, and the boxes represent the modules in each string (11 modules per string).

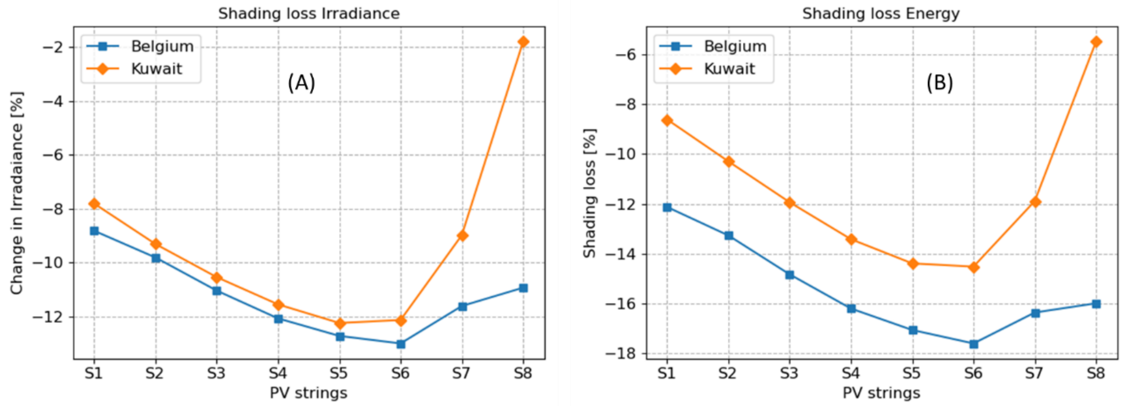

Figure 18. Simulated Irradiance (A) and energy (B) losses due to shading at different strings of the simulated BIPV system.

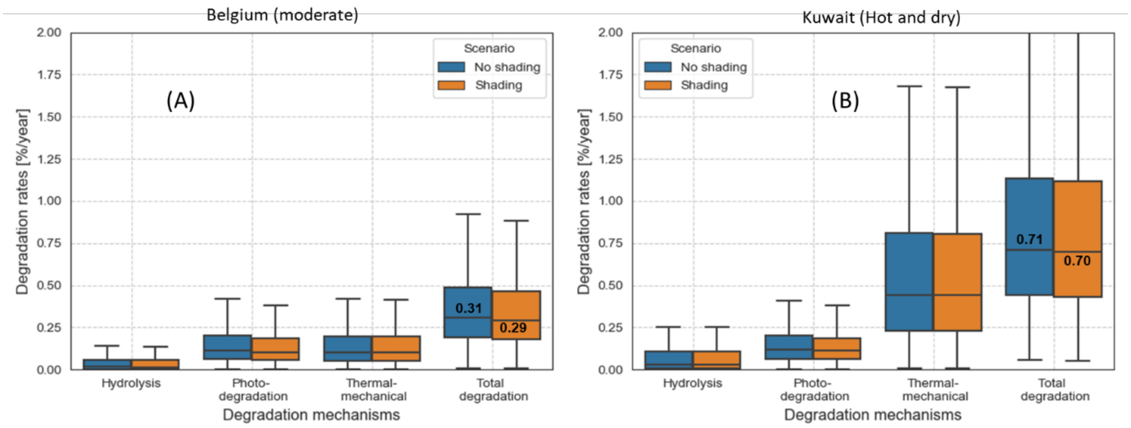

Figure 19. Simulated degradation rates for the different degradation mechanisms and the combined total degradation rate for the No shading and shading scenarios in Belgium (A) and Kuwait (B). The values in the total degradation rate boxplots indicate the median.

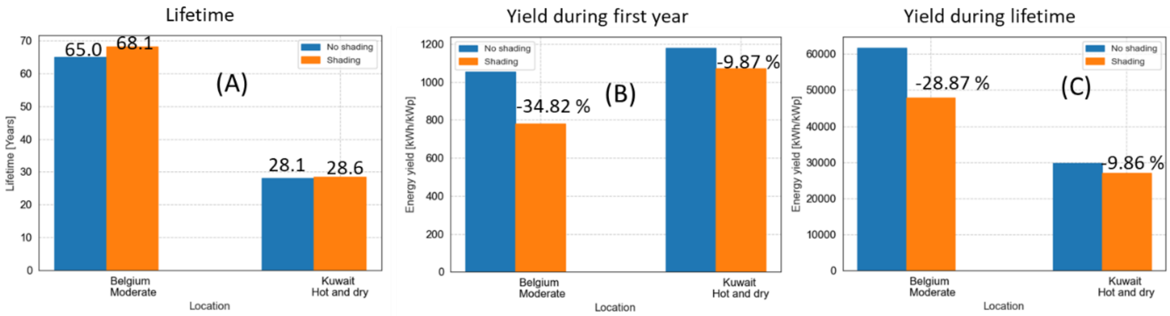

Figure 20. Simulated PV modules lifetime (A), energy yield during the first year (B) and energy yield during the lifetime (C) for the No shading and shading scenarios in Belgium and Kuwait respectively. The values in (A) are estimated lifetime, in (B) and (C) are the energy losses due to shading.

4. Conclusion

Due to their integration, BIPV systems typically function under distinct conditions in comparison to open installation counterparts. The variances in operational conditions could impact PV performance and reliability, with potential positive or negative implications. To accurately assess these implications, a comprehensive simulation framework is essential, considering both performance and reliability aspects. Existing BIPV simulation frameworks often lack reliability models. Therefore, this study introduces a simulation framework focusing on PV modules and inverters, integrating building, energy yield, and reliability models. Validation is conducted using data from a BIPV demonstrator in Belgium.

The proposed BIPV simulation framework is then applied to evaluate the effect of installation designs and shading on the performance and reliability of the BIPV system. The study demonstrates that accurate estimation of the surrounding micro-climate is essential for accurate performance and reliability predictions of BIPV systems, showing significant variations in PV lifetime according to installation and climate. The findings emphasize that despite operating at higher temperatures, properly designed BIPV installations maintain modules lifetimes within warranty periods, attributed to reduced annual irradiation exposure. Additionally, the findings indicate that BIPV systems positively influence inverter reliability compared to their open systems counterparts. Thermomechanical degradation emerges as a prominent mechanism in BIPV systems, influenced by temperature variations and climate.

Finally, the evaluated lifetime benefits due to shading are negligible. The study showed that module performing under constant shading have a small increase in lifetime depending on the climate. The increase in lifetimes for shaded BIPV systems are due to the reduced climate stress factors such as irradiation and temperature. For example, we evaluated annual irradiation reduction of up to ~13 % and ~ 12 % for a BIPV system installed Belgium and Kuwait respectively. Additionally, the average annual module temperature difference between a shaded and unshaded BIPV system was ~1.5°C and 1.2 °C in Belgium and Kuwait respectively. Nevertheless, the extended lifetimes could not compensate for the decrease in energy yield caused by shading.

In essence, this work underscores the importance of considering micro-climate factors in BIPV system modeling to enhance prediction accuracy, and that thoughtful BIPV systems installation design improve system performance, and extend components lifetimes. As future work, the cavity temperature and reliability models could further be improvements to lower the uncertainties in prediction. The thermal models to evaluate the module temperature need to incorporate thermal and optical parameters related to colored PV components to accurately model colored BIPV modules. Additionally, additional degradation models to address various degradation mechanisms, including potential induced degradation (PID), which is particularly relevant in high voltage BIPV systems will be incorporated.

Declaration of Competing Interest

The authors declare that they have no known competing financial interests or personal relationships that could have appeared to influence the work reported in this paper.

Acknowledgements

This work was supported by the DAPPER project, which is financed by Flux50 and Flanders Innovation & Entrepreneurship, Belgium (project number HBC.2020.2144). The authors would also like to thank Jens Moschner and Georgi Yordanov of KU Leuven for their support in BIPV setup data acquisition.

References

[1] A. Ghosh, "Potential of building integrated and attached/applied photovoltaic (BIPV/BAPV) for adaptive less energy-hungry building's skin: A comprehensive review," *J. Clean. Prod.*, vol. 276, p. 123343, Dec. 2020, doi: 10.1016/j.jclepro.2020.123343.

[2] E. Özkalay *et al.*, "Operating Temperatures and Diurnal Temperature Variations of Modules Installed in Open-Rack and Typical BIPV Configurations," *IEEE J. Photovolt.*, vol. 12, no. 1, pp. 133–140, Jan. 2022, doi: 10.1109/JPHOTOV.2021.3114988.

[3] A. W. Fairbrother, A. Virtuani, and C. Ballif, Eds., "Outdoor Operating Temperature of Modules in BIPV and BAPV Topologies," *Proc. EU PVSEC 2020 Online*, 2020, doi: 10.4229/EUPVSEC20202020-6DO.13.3.

[4] M. Muller, J. Rodriguez, and B. Marion, "Performance comparison of a BIPV roofing tile system in two mounting configurations," in *2009 34th IEEE Photovoltaic Specialists Conference (PVSC)*, Jun. 2009, pp. 000817–000822. doi: 10.1109/PVSC.2009.5411159.

[5] C. S. P. López, F. Frontini, G. Friesen, and T. Friesen, "Experimental Testing under Real Conditions of Different Solar Building Skins when Using Multifunctional BIPV Systems," *Energy Procedia*, vol. 48, pp. 1412–1418, Jan. 2014, doi: 10.1016/j.egypro.2014.02.159.

[6] A. Gok, E. Ozkalay, G. Friesen, and F. Frontini, "The Influence of Operating Temperature on the Performance of BIPV Modules," *IEEE J. Photovolt.*, vol. 10, no. 5, pp. 1371–1378, Sep. 2020, doi: 10.1109/JPHOTOV.2020.3001181.

[7] C. Del Pero, N. Aste, F. Leonforte, and F. Sfolcini, "Long-term reliability of photovoltaic c-Si modules – A detailed assessment based on the first Italian BIPV project," *Sol. Energy*, vol. 264, p. 112074, Nov. 2023, doi: 10.1016/j.solener.2023.112074.

[8] A. Fairbrother *et al.*, "Long-Term Performance and Shade Detection in Building Integrated Photovoltaic Systems," *Sol. RRL*, vol. 6, no. 5, p. 2100583, 2022, doi: 10.1002/solr.202100583.

[9] D. C. Jordan, S. R. Kurtz, K. VanSant, and J. Newmiller, "Compendium of photovoltaic degradation rates," *Prog. Photovolt. Res. Appl.*, vol. 24, no. 7, pp. 978–989, 2016, doi: 10.1002/pip.2744.

[10] S. Lindig, J. Ascencio-Vásquez, J. Leloux, D. Moser, and A. Reinders, "Performance Analysis and Degradation of a Large Fleet of PV Systems," *IEEE J. Photovolt.*, vol. 11, no. 5, pp. 1312–1318, Sep. 2021, doi: 10.1109/JPHOTOV.2021.3093049.

[11] A. M. Nobre, S. Karthik, W. Y. Liew, R. Baker, R. Malhotra, and A. Khor, "Performance Evaluation of a Fleet of Photovoltaic Systems Across India and Southeast Asia," in *2019 IEEE 46th Photovoltaic Specialists Conference (PVSC)*, Jun. 2019, pp. 1372–1376. doi: 10.1109/PVSC40753.2019.8981226.

[12] M. Theristis *et al.*, "Onymous early-life performance degradation analysis of recent photovoltaic module technologies," *Prog. Photovolt. Res. Appl.*, vol. 31, no. 2, pp. 149–160, 2023, doi: 10.1002/pip.3615.

[13] A. Louwen, S. Lindig, G. Chowdhury, and D. Moser, "Climate- and Technology-Dependent Performance Loss Rates in a Large Commercial Photovoltaic Monitoring Dataset," *Sol. RRL*, vol. 8, no. 5, p. 2300653, 2024, doi: 10.1002/solr.202300653.

[14] D. C. Jordan, C. Deline, M. Deceglie, T. J. Silverman, and W. Luo, "PV Degradation – Mounting & Temperature," in *2019 IEEE 46th Photovoltaic Specialists Conference (PVSC)*, Jun. 2019, pp. 0673–0679. doi: 10.1109/PVSC40753.2019.8980767.

[15] N. Jakica, R. Young, and J. Eisenlohr, "BIPV Design and Performance Modelling: Tools and Methods: IEA PVPS Task 15, Subtask E, Report IEA-PVPS T15-09: 2019," International Energy Agency, IEA, Report 978-3-906042-86–2, 2019. Accessed: Dec. 14, 2023. [Online]. Available:

https://iea-pvps.org/wp-content/uploads/2020/01/IEA-PVPS_15_R09_BIPV_Design_Tools_report.pdf
[16] R. J. Yang *et al.*, “Digitalizing building integrated photovoltaic (BIPV) conceptual design: A framework and an example platform,” *Build. Environ.*, vol. 243, p. 110675, Sep. 2023, doi: 10.1016/j.buildenv.2023.110675.
[17] T. I. Samarasinghalage, W. M. P. U. Wijeratne, R. J. Yang, and R. Wakefield, “A multi-objective optimization framework for building-integrated PV envelope design balancing energy and cost,” *J. Clean. Prod.*, vol. 342, p. 130930, Mar. 2022, doi: 10.1016/j.jclepro.2022.130930.
[18] H.-J. Kuo, S.-H. Hsieh, R.-C. Guo, and C.-C. Chan, “A verification study for energy analysis of BIPV buildings with BIM,” *Energy Build.*, vol. 130, pp. 676–691, Oct. 2016, doi: 10.1016/j.enbuild.2016.08.048.
[19] J. E. Goncalves, T. van Hooff, and D. Saelens, “A physics-based high-resolution BIPV model for building performance simulations,” *Sol. Energy*, vol. 204, pp. 585–599, Jul. 2020, doi: 10.1016/j.solener.2020.04.057.
[20] J. E. Gonçalves, T. van Hooff, and D. Saelens, “Simulating building integrated photovoltaic facades: Comparison to experimental data and evaluation of modelling complexity,” *Appl. Energy*, vol. 281, p. 116032, Jan. 2021, doi: 10.1016/j.apenergy.2020.116032.
[21] F. Jorissen, G. Reynders, R. Baetens, D. Picard, D. Saelens, and L. Helsen, “Implementation and verification of the IDEAS building energy simulation library,” *J. Build. Perform. Simul.*, vol. 11, no. 6, pp. 669–688, Nov. 2018, doi: 10.1080/19401493.2018.1428361.
[22] H. Goverde, F. Catthoor, V. Dubey, and C. BAERT, “SIMULATION OF PHOTOVOLTAIC MODULES.” Accessed: Dec. 15, 2023. [Online]. Available: https://data.epo.org/publication-server/document?iDocId=5026454&iFormat=0
[23] F. Catthoor, M.-I. BAKA, and P. MANGANIELLO, “SIMULATION OF PHOTOVOLTAIC SYSTEMS.” Accessed: Dec. 15, 2023. [Online]. Available: https://data.epo.org/publication-server/document?iDocId=5026454&iFormat=0
[24] I. Kaaya, M. Köhl, A. Mehilli, S. de C. Mariano, and K. A. Weiss, “Modeling Outdoor Service Lifetime Prediction of PV Modules: Effects of Combined Climatic Stressors on PV Module Power Degradation,” *IEEE J. Photovolt.*, vol. 9, pp. 1105–1112, 2019, doi: 10.1002/pip.2793.
[25] I. Kaaya, J. Ascencio-Vásquez, K.-A. Weiss, and M. Topič, “Assessment of uncertainties and variations in PV modules degradation rates and lifetime predictions using physical models,” *Sol. Energy*, vol. 218, pp. 354–367, Apr. 2021, doi: 10.1016/j.solener.2021.01.071.
[26] “Radiance WWW Server.” Accessed: Dec. 23, 2023. [Online]. Available: https://radsite.lbl.gov/radiance/
[27] A. Alzade and D. Saelens, “Developing a Framework for Automated Modelling of BIPV,” presented at the Building Simulation 2023, in Building Simulation, vol. 18. IBPSA, 2023, pp. 2532–2539. doi: 10.26868/25222708.2023.1508.
[28] H. Montazeri and B. Blocken, “New generalized expressions for forced convective heat transfer coefficients at building facades and roofs,” *Build. Environ.*, vol. 119, pp. 153–168, Jul. 2017, doi: 10.1016/j.buildenv.2017.04.012.
[29] I. T. Horváth *et al.*, “Photovoltaic energy yield modelling under desert and moderate climates: What-if exploration of different cell technologies,” *Sol. Energy*, vol. 173, pp. 728–739, Oct. 2018, doi: 10.1016/j.solener.2018.07.079.
[30] I. Kaaya, D. Mansour, P. Gebhardt, K. Weiß, and D. Philipp, “Modelling and Validation of Photovoltaic Degradation under Ultraviolet-Damp-Heat Conditions,” *2021 IEEE 48th Photovolt. Spec. Conf. PVSC*, 2021, doi: 10.1109/PVSC43889.2021.9519050.
[31] “scipy.stats.ncf — SciPy v1.11.1 Manual.” Accessed: Jul. 05, 2023. [Online]. Available: https://docs.scipy.org/doc/scipy/reference/generated/scipy.stats.ncf.html
[32] S. Lindig, I. Kaaya, K.-A. Weiß, D. Moser, and M. Topic, “Review of Statistical and Analytical Degradation Models for Photovoltaic Modules and Systems as Well as Related Improvements,” *IEEE J. Photovolt.*, vol. 8, no. 6, pp. 1773–1786, Nov. 2018, doi: 10.1109/JPHOTOV.2018.2870532.
[33] M. Koehl, M. Heck, and S. Wiesmeier, “Categorization of weathering stresses for photovoltaic modules,” *Energy Sci. Eng.*, vol. 6, no. 2, pp. 93–111, 2018, doi: 10.1002/ese3.189.
[34] M. Owen-Bellini, “Thermomechanical degradation mechanisms of silicon photovoltaic modules,” thesis, Loughborough University, 2017. Accessed: Dec. 29, 2023. [Online]. Available: https://repository.lboro.ac.uk/articles/thesis/Thermomechanical_degradation_mechanisms_of_silicon_photovoltaic_modules/9539651/1
[35] U. Eitner, “Thermomechanics of photovoltaic modules,” 2011, doi: 10.25673/529.

[36] A. Ristow, M. Begovic, A. Pregelj, and A. Rohatgi, “Development of a Methodology for Improving Photovoltaic Inverter Reliability,” *IEEE Trans. Ind. Electron.*, vol. 55, no. 7, pp. 2581–2592, Jul. 2008, doi: 10.1109/TIE.2008.924017.
[37] F. Chan and H. Calleja, “Design Strategy to Optimize the Reliability of Grid-Connected PV Systems,” *IEEE Trans. Ind. Electron.*, vol. 56, no. 11, pp. 4465–4472, Nov. 2009, doi: 10.1109/TIE.2008.928100.
[38] “MIL-HDBK-217 F RELIABILITY PREDICTION ELECTRONIC.” Accessed: Mar. 29, 2024. [Online]. Available: http://everyspec.com/MIL-HDBK/MIL-HDBK-0200-0299/MIL-HDBK-217F_14591/
[39] X. Shi and A. M. Bazzi, “Solar photovoltaic power electronic systems: Design for reliability approach,” in *2015 17th European Conference on Power Electronics and Applications (EPE’15 ECCE-Europe)*, Sep. 2015, pp. 1–8. doi: 10.1109/EPE.2015.7309352.
[40] Y. Yang, V.-S. Sularea, K. Ma, and F. Blaabjerg, “Advanced design tools for the reliability of power electronics — Case studies on a photovoltaic (PV) system,” in *IECON 2015 - 41st Annual Conference of the IEEE Industrial Electronics Society*, Nov. 2015, pp. 002828–002833. doi: 10.1109/IECON.2015.7392531.
[41] V. Smet *et al.*, “Ageing and Failure Modes of IGBT Modules in High-Temperature Power Cycling,” *IEEE Trans. Ind. Electron.*, vol. 58, no. 10, pp. 4931–4941, Oct. 2011, doi: 10.1109/TIE.2011.2114313.
[42] P. Ghimire, A. R. de Vega, S. Beczkowski, B. Rannestad, S. Munk-Nielsen, and P. Thogersen, “Improving Power Converter Reliability: Online Monitoring of High-Power IGBT Modules,” *IEEE Ind. Electron. Mag.*, vol. 8, no. 3, pp. 40–50, Sep. 2014, doi: 10.1109/MIE.2014.2311829.
[43] Y. Yang, A. Sangwongwanich, and F. Blaabjerg, “Design for reliability of power electronics for grid-connected photovoltaic systems,” *CPSS Trans. Power Electron. Appl.*, vol. 1, no. 1, pp. 92–103, Dec. 2016, doi: 10.24295/CPSSTPEA.2016.00009.
[44] “Intelligent Power and Sensing Technologies | onsemi.” Accessed: Dec. 21, 2023. [Online]. Available: https://www.onsemi.com/
[45] S. Bouguerra *et al.*, *Reliability Analysis and Energy Yield of a String Inverter for a BIPV Application considering the Cavity Temperature Measurements*. 2023. doi: 10.13140/RG.2.2.12917.55529.
[46] M. Matsuichi and T. Endo, “Fatigue of metals subjected to varying stress,” 1968. Accessed: Mar. 28, 2024. [Online]. Available: https://www.semanticscholar.org/paper/Fatigue-of-metals-subjected-to-varying-stress-Matsuichi-Endo/467c88ec1feaa61400ab05fbe8b9f69046e59260
[47] U. Scheuermann and R. Schmidt, “Impact of load pulse duration on power cycling lifetime of Al wire bonds,” *Microelectron. Reliab.*, vol. 53, no. 9, pp. 1687–1691, Sep. 2013, doi: 10.1016/j.microrel.2013.06.019.
[48] S. Bouguerra, M. R. Yaiche, O. Gassab, A. Sangwongwanich, and F. Blaabjerg, “The Impact of PV Panel Positioning and Degradation on the PV Inverter Lifetime and Reliability,” *IEEE J. Emerg. Sel. Top. Power Electron.*, vol. 9, no. 3, pp. 3114–3126, Jun. 2021, doi: 10.1109/JESTPE.2020.3006267.
[49] “JRC Photovoltaic Geographical Information System (PVGIS) - European Commission.” Accessed: Apr. 03, 2023. [Online]. Available: https://re.jrc.ec.europa.eu/pvg_tools/en/#TMY

Appendix

A. Irradiance profiles for a BIPV module in different locations

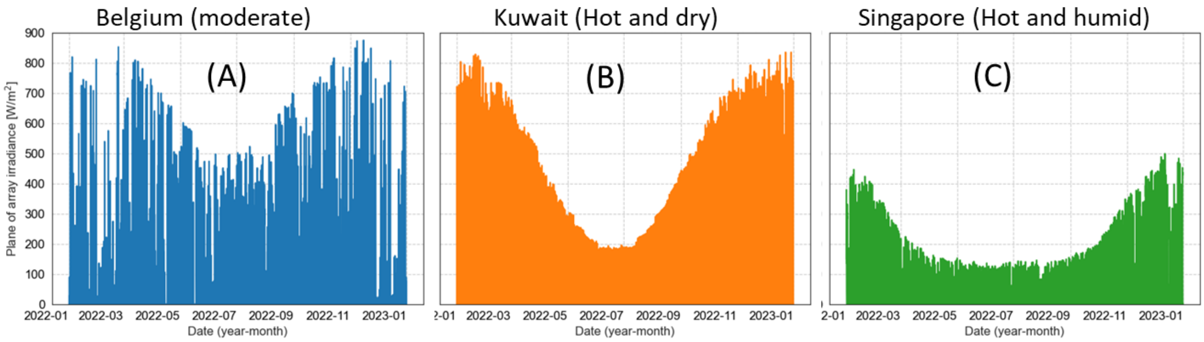

Figure A 1. Simulated plane of array irradiance profiles for a vertical BIPV in different locations.

B. Mechanical simulation details

The PV module assumed is constituted of 16 5-busbar Passivated Emitter Rear Contact (PERC) cells (4x4), four layers of Thermoplastic Polyolefin (TPO) encapsulant (two on the front and two on the back), and two glass-sheets. All the dimensions are described in Table B 1 and the geometry considered for the FEM simulation is visualized in Figure B 1. Only half of the PV module is visible since symmetry conditions were applied, for faster computation.

Table B 1. Dimensions of all the components included in the studied PV module.

Component	Dimensions
Glass	1000 mm x 1000 mm x 4 mm
Encapsulant (TPO)	1000 mm x 1000 mm x 0.5 mm
Cell	158.75 mm x 158.75 mm x 0.18 mm
Edge gap	115 mm
Cell gap	45 mm

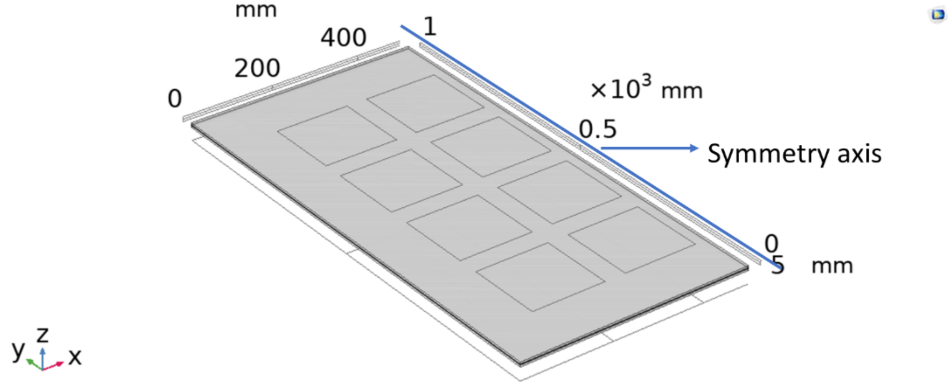

Figure B 1 Geometry of the global-approach study representing half of the simulated PV module. The symmetry axis is demonstrated by a blue line.

The PV module is attached within a wooden frame by rubber. This type of attachment keeps it in place while providing the capability of limited expansion. To replicate this specific type of attachment in COMSOL Multiphysics, rollers were used as boundary conditions (Figure B 2), one for each of the three attached sides (symmetry condition was applied on the fourth one). The rollers were limiting, without prohibiting, the lateral movements (x-y axes) of the PV module, while allowing perpendicular movements (z axis). However, the PV module's perpendicular movement was constrained at the edges due to the rubber, so two additional roller cylinders along the y axis were assumed, one on the top glass and one on the bottom, with x coordinate 3 mm (Figure B 2).

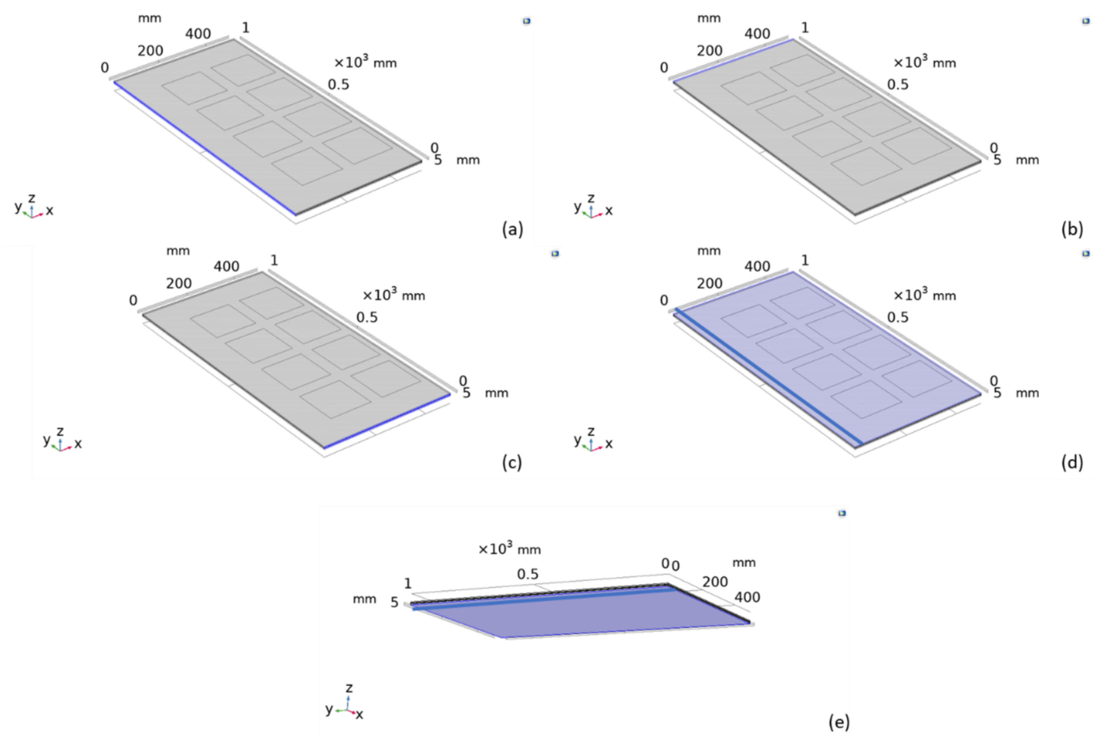

Figure B 2. (a-e) All the boundaries of the geometry where rollers were applied.

For the estimation of the thermomechanical stress on the ribbons, solder and interconnections, the global-to-local approach is utilized. According to it, a specific part of the full geometry is selected, which includes the ribbons, solder, and interconnection between two cells. For the present example, the studied geometry belongs to the cells indicated in Figure B 3 on the first busbar (at 130.375 mm from the edge of the PV module). The dimensions of the ribbon and solder's cross-sections were 1 mm x 0.2 mm and 1mm x 0.02 mm respectively. The solder was assumed to start at 1 mm from the edge of the PV cells (Figure B 3C). The displacement of the glass calculated from the global model was applied as a boundary condition for the local model.

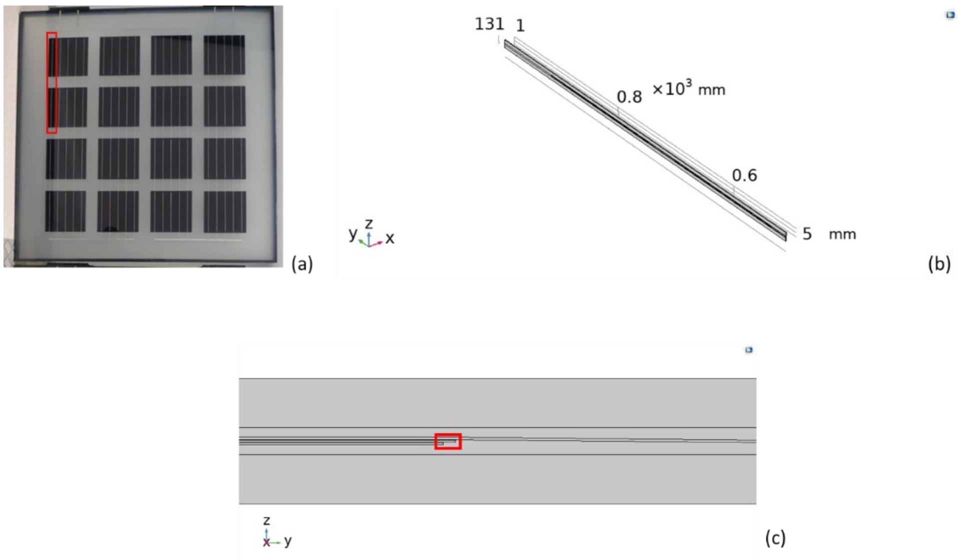

Figure B 3. (a) The real PV module where the studied region for the local approach is indicated in a red rectangle. (b) Geometry for the local approach. (c)Cross-section of the geometry for the local approach. The red rectangle indicates the initiation of the solder.

All the materials have been modeled as linear elastic except the encapsulant, which has been considered viscoelastic, and the solder which has been assumed to be a viscoplastic material. The physics applied on the PV modules were thermal expansion and gravity. Table B 3 summarizes the material properties for each component with reference temperature 20 °C, which were received according to the COMSOL Multiphysics material library and other sources [34], [35]. The encapsulant's material properties were assumed to be the same as these for an Ethylene Vinyl Acetate (EVA) encapsulant, due to literature availability. Time-dependent properties are not included in the table since all the studies were stationary. The mesh of the global model was normal, while a more detailed mesh was selected for the local approach, including finer tetrahedral for the solder, normal tetrahedral for the glass and fine tetrahedral for the rest of the model.

Table B 2. Material properties utilized for all thermomechanical simulations.

Material	Young's Modulus, E (Pa)	Poisson's Ratio, v	Density, ρ (kg/m^3)	Thermal Expansion Coefficient, α (1/K)
Glass	$73•10^9$	0.40	2500	$8.0•10^{-6}$
Cells	$170•10^9$	0.28	2329	$2.6•10^{-6}$
Encapsulant	$5.6•10^6$	0.40	960	$2.7•10^{-4}$
Ribbons	$110•10^9$	0.35	8960	$17•10^{-6}$
Solder	$10•10^9$	0.40	9000	$21•10^{-6}$

Table B 3.. Studied regions for stress evaluation.

	X (mm)	Y (mm)
Cell (centre)	597-607 and 801-811	5-5.18
Cell (edge)	679.25-681.25 and 726.25-728.25	5-5.18
Solder	679.25-680.25 and 727.25-728.25	5.18-5.2 and 4.98-5

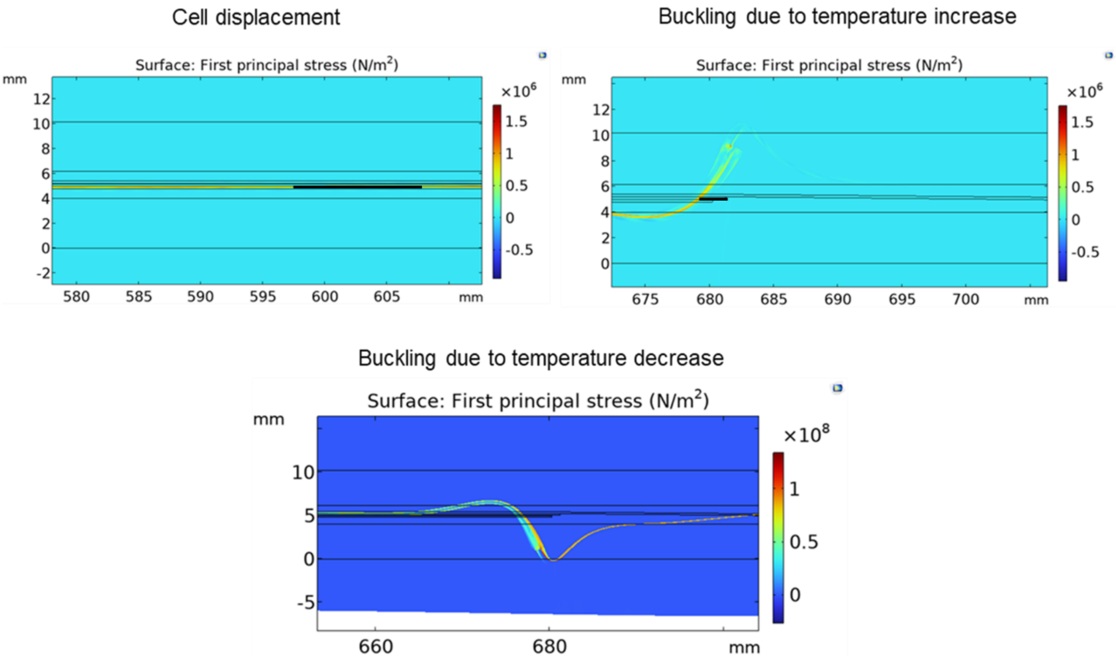

Figure B 4. Representations of the cell displacement (cell center) and buckling effects due to temperature increase and decrease. All the representations are magnified for visibility. The dark black lines indicate the studied regions of the cell, described in Table B 3. For the buckling effect, the solder region studied was the one above the black line.